ACQUISITION OF ICE PROPERTIES USING MECHANICAL ACTUATION

MICHAEL C. WRINCH

Acquisition of Ice Properties Using Mechanical Actuation

by
©Michael C. Wrinch

A thesis submitted to the School of Graduate Studies
in partial fulfillment of the requirements for the
degree of Master of Engineering

Faculty of Engineering and Applied Science
Memorial University of Newfoundland
2002

St. John's Newfoundland Canada

Abstract

Research surrounding acoustic resonance properties of ice has increased and now a practical method for depth profiling has been developed. Experiments were performed in real-time with high sensitivity, biaxial, wide bandwidth accelerometers (10 KHz bandwidth), which encompassed a high sampling rate of 200 Kb/sec/channel with a 12-bit resolution (36 dB). The implementation of signal processing produced a seismic and resonant signature. Initially repeated results revealed an accurate correlation between ice depth to its characteristic frequency. The required velocity was determined using the time of arrival and the cross-correlation between transducers. Theoretical analysis has indicated that the system will be capable of resolving values close to the theoretically calculated error of less than 6 %: this device therefore can be readily realized as a compact portable field instrument.

Acknowledgments

Much thanks is extended to the Memorial University of Newfoundland Faculty of Engineering and Applied Science who provided the opportunity to conduct this work. Particularly, Dr. Mary Williams and Dr. Siu O'Young who consistently offered both positive and professional support throughout my research. The expertise they have provided in each of their specific fields has been an invaluable reference. Additionally, the editing of this thesis was conducted by Julia Kiernan, who's grammatical skills were a great help.

The staff at the Institute for Marine Dynamics (IMD) in St. John's, Newfoundland were a very helpful reference. The lab technician's knowledge of the electronics regarding robust packaging, electronic systems, and layout are superior to persons previously encountered. Similarly, the ice tank support staff were always available for a quick reference to eliminate any possible problems.

Technical services in the department of Applied Science and Engineering at Memorial University of Newfoundland were also of great assistance. All of the jobs that they conducted were of high quality and were efficiently completed in all departments. Dr Neil Bose of the department of Naval Engineering at Memorial University of Newfoundland was a tremendous aid concerning the development of the transducer's mechanical design and regarding methods of calibration. The final department to mention is the department of Geology and Geophysics at Memorial University of Newfoundland, they proved to be a vast and direct reference of information pertaining to seismology and geophone technology.

In closing, this work could not have been completed without the support from my aunt and uncle, Marcel and Mary Mondou, who kept me healthy. I would also like to thank my closest collegues Lloyd Smith and Jagan Seshadri who inspired and motivated me on the days when I felt lost. Most importantly, they taught me the

skill of remaining relaxed while maintaining discipline. Finally, I would like to thank my parents who have helped support me and who been extremely patient with my erratic behavior.

Contents

List of Tables

List of Figures

Chapter 1

Introduction

1.1 Research Rationale

The purpose of this thesis is to prove and demonstrate that seismic and resonance methodology is a viable technique for determining ice depth. The problem statement concerns determining specific ice properties, such as the depth, using acoustic sensing on ice sheets while developing cost effective, precision instrumentation to conduct the experiments. A possible setup proposed can be seen in Figure: 1.1 and Figure: 1.2.

Through development in the areas of both computer hardware and software the less invasive methods of ice profiling, which were only theoretically possible, are now practically achievable using seismic and resonant techniques. The first is a small scale seismic technique which measures the time from an initial excitation pulse to the first reflection. The second method matches the resonant characteristics of an ice sheet to its geometric dimensions. Although both methods are theoretically straightforward, instrumentation challenges manifest in the collection of data at sufficiently high sampling speeds, verifying transducer precision, ensuring suitable wide bandwidth in the actuators, and minimizing the signal to noise ratio.

Rapid, low cost ice thickness profiles are required for transportation, safety, and environmental applications. Ice thickness information assists ships in route planning when navigating in ice covered waters. Thick ice may pose a hazard for offshore drilling, while thin ice is dangerous in areas where the ice surface is used for ice roads and snowmobiles. Since the heat budget of the ocean is highly correlated with

the thickness of the ice cover. ice thickness is also a sensitive measure of global warming. Though modern ice profiling methods have been developed. direct measurement through drilled holes remains most common due to its simplicity. cost. and accuracy.

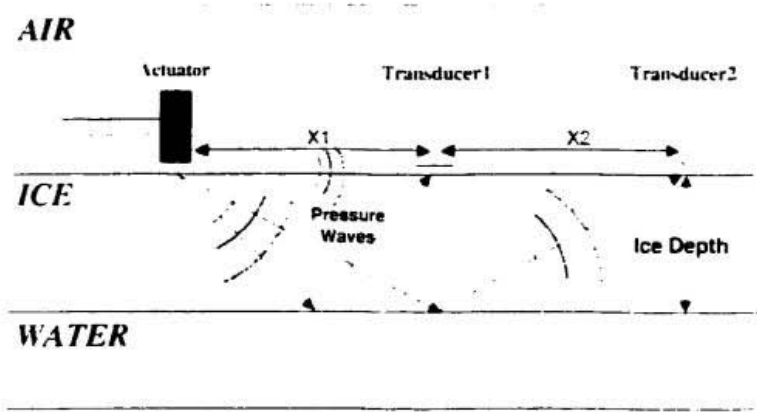

Figure 1.1: Possible Setup Using Time Analysis

1.2 Previous Work

In previous reports. [1] [2] acoustic analysis of ice depth was said to be feasible despite the fact that experimentation has only been attempted in a very rudimentary form. In 1969. Langleben [3] claimed that due to the lack of precision instruments. this type of experimentation was impossible. However. thirty years later. instrument technology has progressed to the point that acoustic measurements can be made with the needed precision.

Before this investigation could be conducted a review of the previously published work : (a) actuators styles. (b) vibration characteristics. (c) modulus. (d) sound velocity. and (e) attenuation/meter has been carried out.

The field of ice acoustics and seismology can be divided into a series of areas including ice noise. ice properties. and seismic techniques. Although there is no published research directly involved with the resonance of ice sheets. there is significant data which suggests that this technique is a possible method for determining

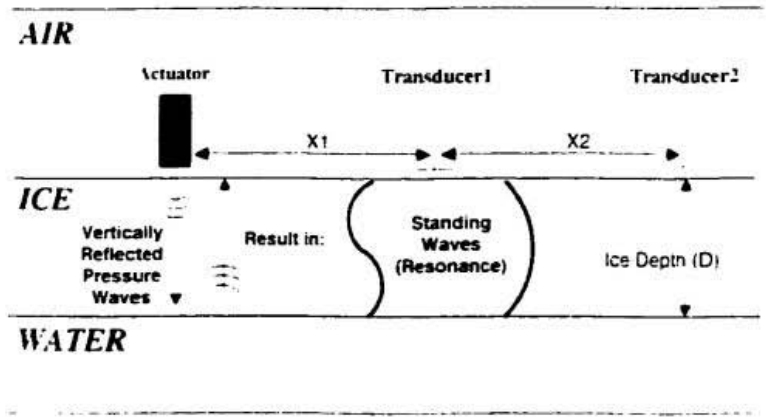

Figure 1.2: Possible Setup Using Ice Resonance

ice sheet depth [4], [5]. The theory will be presented mathematically in Chapter 2. In the following sections, a qualitative investigation of past research concerning ice acoustics and relevant topics will be addressed.

1.2.1 Properties of Ice

Ice properties frequently measured are Young's modulus E [6] [7], acoustic velocity (P and S waves), density and acoustic attenuation. Frankenstein [8] explains that Young's modulus is dependant on P-wave velocity and ice density $c_o = (\frac{E}{\rho})^2$. Also velocity and P-wave are both, in part, dependant on salinity and temperature [8]. In his experimentation Frankenstein used piezoelectric transmitters and receivers connected to an oscilloscope where this device was tuned to 20 KHz in order to measure the velocities in differing types of ice bars (i.e. different salinity, temperature and orientation). This experiment determined velocity to obtain the modulus from Equation 1.1 and c is the velocity, E is Young's modulus, and ρ is the density.

$$c = (\frac{E}{\rho})^2 \tag{1.1}$$

With the data collected, an equation of horizontal velocity for columnar ice (Equation 1.2) and an equation for vertical velocity in granular ice (Equation 1.3) was

determined. These equations can be related to relations of Young's modulus of brine filled ice. Additionally, Williams [6] discusses a very similar methodology for determining E where the experimental methodology is very similar to Frankenstein's work.

$$E = (9.88 - 0.29 \cdot \upsilon_h) GN/m^2 \tag{1.2}$$

$$E = (11.8 - 0.002 \cdot \upsilon_v) GN/m^2 \tag{1.3}$$

The variable υ in Equations 1.2 and 1.3 is defined as ppt salinity parts per thousand.

Ringer's [9] investigations into ice properties used a similar setup as the previously outlined methods, the difference being the implementation of both fresh and methanol "doped" ice. In this experiment, the signal was received and transmitted with Hoffrel 310A transducers at a carrier frequency of 2 MHz. The results obtained were an undoped ice velocity of 3780 m/s, and $E = 8.60 GN/m^2$, whereas for the doped ice, the velocity was measured at 1700 m/s and $E = 1.5 GN/m^2$.

Alphonso [10] measured the acoustic wave velocity of undoped ice by placing $3.25 \cdot 10^{-3}$ m ice sheets in between aluminum plates using a pulse frequency of 5 MHz at -26 °C, and found values of $\rho = 0.9168 g/cm^{-3}$ $V_{compressional} = 3940 m/s$ and $V_{shear} = 1990 m/s$. All of the values determined in lab and actual experimental settings reveal a consistent result for velocity and density values, meaning that this technique is an effective method for determining ice velocity.

An additional area of interest with ice acoustics is cross-crystal sound attenuation. This concept is important to seismic and resonance calculations because a signal must travel through the ice sheet. During this passage it may travel through multiple reflections before returning to transducers, therefore the attenuation/meter/Hz of ice in conjunction with the sensitivity limit of a transducer will limit the resolvable depth of ice. Nevertheless, if ice depths of 0.10 m to 10 m were measured then using Equation 1.6, previously determined velocities and densities, the frequency ranges are found to be between 0.15 KHz and 20 KHz. What remains to be solved is the signal attenuation in these frequency ranges.

Of the three papers reviewed, the signal loss below 20 KHz was also below 1.5 dB/m. Langleben [11] determined that a signal loss in the cores of sea ice and glacier ice to be less than 1.5dB/m at 20 KHz and a signal loss of over 8dB/m above 200 KHz: this signal followed equation 1.4. Other experiments, such as Bogorodskii's [12] work of attenuation of sound above 100 KHz, demonstrate that if the attenuation above 100 KHz is projected to 0 KHz, the attenuation would approach 0dB/m. The slope extrapolated followed the Equation 1.5. In Equations 1.4 and 1.5, α is the attenuation, f is the frequency, and c_x is a constant determined from the graphical fit of the data.

$$\alpha = c_1 f + c_2 f^4 \tag{1.4}$$

$$\alpha = c_1 f + c_2 f^2 \tag{1.5}$$

Another experiment by Langleben [3], approaches transmission coefficients of ice-water boundaries at different angles. At frequencies less than 17 KHz, the reflection coefficient of the ice-water boundary was found to be no less than 20% measured at angles as small as 15° and up to 75° where the reflection coefficient was as high as 80%. This experiment was conducted by placing a hydro-actuator and a hydrophone through two separate holes in an ice sheet. The the actuator "pinged" up at the ice while the hydrophone received the signal and calculated the loss of energy, however, it should be noted that the calibration techniques were not referred to.

1.2.2 Ice Noise

Ice noise, specifically ice cracking, contains an immense amount of acoustic information [13] [14] . Large quantities of data have been collected and have been used for determining information about ice's characteristics. For example, work by Farmer and Xie [5] consisted of placing 20 KHz bandwidth hydrophones below first year sea ice and then leaving the ice to drift and break up while recording the cracking noise. High frequency components were discovered and in particular, a peak near the fundamental frequency of the ice-air ice-water resonance was recorded of 5 KHz. The fundamental frequency was proven through the wave equation as stated

by Frankenstein [8]:

$$f_{res} = \frac{V_{ice}}{2 \cdot depth_{ice}} \tag{1.6}$$

Information relating to large low frequency components, wind interaction, and water interactions were correlated with the ice's surface cracking. Other examples of acoustical emissions and microcracking measurements are published by Sinha [14]. His experiment determined that acoustical emissions were able to be implemented as a scale for measuring the state of ice under compression, however, it should be noted that these experiments were conducted in a laboratory setting.

Other researchers who conducted experiments in the collection of ice noise include Gavirlo and Gusev. Their experiments dealt with the concept that the noise in ice was created using surface impactors. Gavrilo and Gusev [15] conducted experiments where snow covered ice was treated with three different impactors. The three apparatus used were a plate, a rod, and a parallelepiped. The testing took place on a snow covered lake ice after a spell of low temperatures (-20 to -30 C); the lake was 3 to 3.5m deep and the experiments were 350 m from shore. The measurements were recorded using contact vibrographs and hydrophones suspended below the ice. The information collected showed that impact durations that lasted approximately 0.02 seconds. The modulus of the ice being $9.5MN/m^2$, the velocity of the P-wave 3200 m/s, and having a varying natural frequency 0.050 to 1.0 KHz. Ice sheet depths were not recorded.

1.2.3 Seismic Techniques, Transducers, and Actuators

Techniques

Seismic Reflection Profiling (SRP) is a commonly used technique for viewing underground rock structures through sound wave manipulation. Widely used by geoscientists, it plays an important role in oil exploration. SRP can be performed on either land or sea. Below in Figure 1.3 is a marine example of SRP. A sound wave (red line) is created by an "air gun" on the boat. The vibrations travel in the water (blue) and penetrate into the layers of sediments (light brown) and rocks

(dark brown) that make up the ocean floor. Parts of this sound reflect off the different layers, and consequently travel back up to the sea surface where they are recorded by the hydrophones (black bar) which are dragged behind the ship. *reference: (http://rainbow.ldeo.columbia.edu/ees/lithosphere/sonar/sonar.html).*

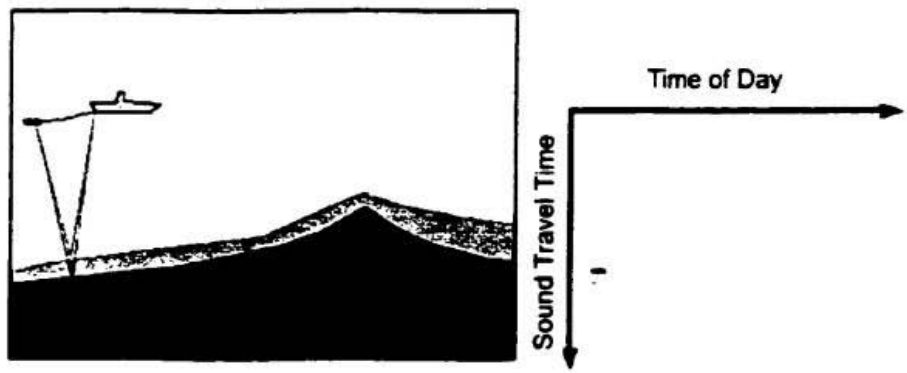

Figure 1.3: Seismic Sonar Example

Another technique of measurement is refraction. A wave travelling through one medium intersects a change of medium (i.e. sand stone to marble) at its critical angle resulting in a wave which travels along the material boundary. The critical angle is then determined using Snell's Law of Refraction:

$$\frac{sin(\theta_1)}{V_1} = \frac{sin(\theta_2)}{V_2} \tag{1.7}$$

For example, where layers of granite rock end and a layer of sandstone layer begins, an impact wave could travel along the sand-granite boundary. However, this technique is only useful when the separation distance of source to receiver is high [16].

Impactors and Receivers

Seismic signals are produced using a series of different techniques. Examples listed by Sheriff in [16] are:

- Buffalo gun

- Sledge Hammer
- Bean Bag (136 KG weight dropped from 3 m)
- Hydraulic hammer
- 1 KV Piezo electric stack
- Explosives
- Air Gun

Yet this does not answer how vibrations are received. Historically, the most common receivers are geophones that consist of either moving coil electromagnetics, capacitance, or variable-reluctance devices. However, for smaller scale vibrations (i.e. the automotive industry), other types of devices such as piezoelectric, strain gauges, laser vibrometers, fiber optic transducers, and solid state silicone sensors (micro-machines) [17] are available. These smaller devices have the advantage of a larger frequency response and higher sensitivity.

Experiments

Upon review of the basic seismic techniques, some research concerning the scope of this thesis is that of Xiang [18] and Farmer [4]. Xiang's thesis compared impulsive and vibrator sources that are portable and applicable for near-surface high resolution seismic studies. An emphasis was placed on the frequency spectrum and on energy levels in the attempt to improve resolving power. The key element of Xiang's analysis was an inverse convolution that determined the transfer function of the rock. The published findings of Farmer show that experiments were conducted using a 3.6 kg hammer on 1.75 m thick first-year ice 100 m from the four vertically hanging hydrophones, 5 m to 70 m below the ice. The result was a natural frequency of 0.516 KHz, and the P-wave velocity was 2630 m/s. He took these experimental values and used Equation 1.6 which does not correlate to the depth of 1.75 m but 2.54 m.

1.3 Acoustical Ice Depth Measuring Products Available

Currently, three companies, ASL Environmental Sciences, Polar Tech Ltd. and Canpolar Consultants Ltd have investigated this particular type of measurement. The first, ASL Environmental Sciences, is located in Sidney, British Columbia, Canada. ASL's device, The Ice Profiler, is placed on the bottom of the ocean for periods of up to 6 months. The profile of the ice floe over the top is then tracked using ultrasonic acoustical pulses. Once the desired data has been collected, the device is retrieved from the ocean floor and the data can be downloaded to a computer. This device is currently in use today.

The second company Polar Tech Ltd. no longer exists. However, their product, the Portable Acoustic Thickness Sensor (PATS), is capable of determining ice sheet depth. It consists of an electronic acoustical actuator, three accelerometers and a very simple computer. The device would "chirp" the ice with its actuator and then receive the data at the three accelerometers. However the algorithm was not public, but the device would require over eight minutes to make each measurement.

Finally, the third company reviewed, Canpolar Consultants Ltd. has not produced any ice characteristic measuring instruments, but Canpolar Consultants has suggested alternative opportunities available. Canpolar Consultants' report, titled "Review of Floating Ice Thickness Measurement Capability, Technologies and Opportunities" was prepared for the Canadian Department of Fisheries and Oceans in January of 1985. The three possible methods for measuring ice thickness suggested are radar pulses (SAR), acoustical resonance, and acoustical time of reflection.

1.4 Technical Difficulties

The technical difficulties discovered from this literature and theoretical review are with instrumentation, and computer equipment. Common to all previous investigations in ice acoustics, hydrophones were used. However, hydrophones are not useful for this experiment because drilling into the ice will defeat the non-invasive investigation's purpose. Additionally, the main difficulty with geophones is that they are not designed for the high frequency sensing [16]. Other challenges have been instrument

signal saturation as is seen with Xiang's [18] and Farmer's [4] experimentation. This limitation has made transfer function ($h(t)$) investigations extremely difficult. The final limiting technical difficulty to overcome is low computer sampling rates.

1.5 Scope of Thesis

The possibilities surrounding the investigation of this topic are vast, and a narrowing of the field was necessary. The target goals accomplished in this investigation are to:

1. Mathematically prove that ice resonance and time reflections are a viable method to determine ice properties.
2. Develop a method of instrumenting ice vibrations.
3. Create software for the data acquisition system.
4. Collect experimental data on actual ice.
5. Develop a functioning algorithm to automatically calculate ice properties.

Chapter 2

Theoretical Background and Feasibility

Interpreting the depth of ice using acoustic resonance and timing reflections requires some prior knowledge of geoscience and signal processing. In order to prove that ice depth can be determined using acoustics, a theoretical feasibility will be conducted in this chapter, beginning with a physical description of waves in solids, followed by an explanation of signal processing techniques needed, and ending with some specific feasibility calculations.

2.1 The Wave Equation and Wave Propagation

In an elastic solid, the two types of deformations which result from an external force are compression and shear. From the elasticity and dynamics theories, the deformations result in two principal independent wave propagations where the first and fastest forces are compressional waves (p-waves) and the slower forces are shear waves (s-waves). The wave equation is derived from Newton's Second Law of Motion which states that an unbalanced force on a mass produces acceleration ($F = ma$). Assuming that we are dealing with an isotropic material, in similar terms, when the properties of the material do not depend on orientation, the wave equation can then be expressed in the Equations 2.1 and 2.2. In the following equations, Δ is the dilational potential $\varepsilon_{xx} + \varepsilon_{yy} + \varepsilon_{zz}$ and Θ is the rotational vector potential.

$$\nabla^2 \Delta = \frac{1}{\alpha^2} \frac{\partial^2 \Delta}{\partial t^2} \tag{2.1}$$

$$\nabla^2\Theta = \frac{1}{\beta^2}\frac{\partial^2\Theta}{\partial t^2} \tag{2.2}$$

α and β are constants of p and s wave velocities equaling V_p and V_s respectively. Furthermore, each wave V_p and V_s can be further defined in equations 2.3 and 2.4, where the variables λ and μ are the Lamé's elastic constants which completely specify the nature of an isotropic solid [19].

$$V_p = \sqrt{\frac{\lambda + 2\mu}{\rho}} \tag{2.3}$$

$$V_s = \sqrt{\frac{\mu}{\rho}} \tag{2.4}$$

V_p and V_s indicate that the compressional wave will always be faster than the shear wave. It is important to note that shear waves do not exist in liquid mediums. However, from these two velocities, the elastic constants of ice, Young's Modulus, E, and Poisson's Ratio, σ, may be found from Equations 2.5 and 2.6.

$$E = \frac{\mu(3\lambda + 2\mu)}{\lambda + \mu} \tag{2.5}$$

$$\sigma = \frac{\lambda}{2(\lambda + \mu)} \tag{2.6}$$

Dividing β in to α (Equation 2.7) results in a reduction in a form where if σ, Poisson's ratio, decreases from it's maximum of 0.5 to 0, the ratio will then increase from 0 to $1/\sqrt{2}$. In other words, V_s can never be greater than 70 % of V_p. Experimentally, both waves will be viewed, yet the wave of interest is the compressional wave, V_p.

$$\frac{\beta}{\alpha} = \sqrt{\frac{\mu}{\lambda + 2\mu}} = \sqrt{\frac{0.5 - \sigma}{1 - \sigma}} \approx \sqrt{\frac{1}{3}} \tag{2.7}$$

2.1.1 Huygen's Principle

In an isotopic wavefront from a point source, Huygen's Principle states that every point on the wavefront can be regarded as a new source of wave activity. The physical

rationale behind this is that (a) each particle located on a wavefront has moved from its equilibrium position in. approximately. the same manner. (b) the elastic forces on neighboring particle are thereby changed. and (c) the resultant of the changes in force due to the motion of all the points on the wavefront produces the motion that forms the next wavefront [16]-p.44. Hence. Huygen's Principle is useful for predicting the future positions of wavefronts.

2.1.2 Snell's Law

When wavefronts reach a homogeneous surface boundary. part of the wave energy is reflected and part of the wave energy is transmitted. As well. the ray paths are bent according to Snell's Law as outlined in Figure 2.1 and equation 2.8. At some incidences. there is a critical angle in which all the incident energy is reflected. This is known as the *critical angle*: however. because water has a slower P-wave velocity than ice (~1400 m/s vs ~3800m/s) there is no critical angle for an ice-water boundary.

$$\frac{sin(\theta_1)}{V_{P1}} = \frac{sin(\theta_2)}{V_{P2}} \tag{2.8}$$

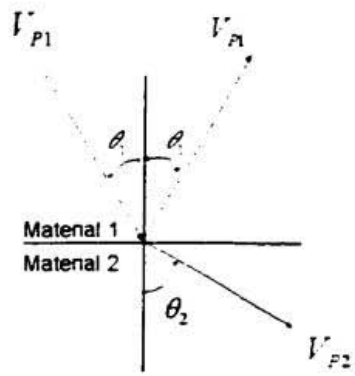

Figure 2.1: Snell's Law

In the case of a normal incidence with a boundary ($\theta = 0$). the reflection and transmission coefficients (R and T). derived from the Zoeppritz equations. are stated in Equation 2.9 for reflection Equation and 2.11 for transmission. Z_1 and Z_2 are the

characteristic impedances of each material where $Z_x = \rho_x V_x$ and the reflected energy and transmitted energy are obtained from Equations 2.10 and 2.12. To calculate use these formulas. Z_2 refers to the medium the wave in Z_1 is about to enter into. Additionally, E_R and E_T are normalized meaning that $E_R + E_T = 1$.

$$R = \frac{Z_2 - Z_1}{Z_2 + Z_1} \tag{2.9}$$

$$E_R = (\frac{Z_2 - Z_1}{Z_2 + Z_1})^2 = R^2 \tag{2.10}$$

$$T = \frac{2Z_1}{Z_2 + Z_1} \tag{2.11}$$

$$E_T = \frac{4Z_2Z_1}{(Z_2 + Z_1)^2} = \frac{Z_2}{Z_1}T^2 \tag{2.12}$$

2.1.3 Fresnel Zone

Horizontal timing resolution is limited by the size of the first Fresnel zone [16]. As seen from Huygen's principle, points on a wave front are sources of secondary wave fronts. Therefore, the reflected energy viewed by a transducer on an ice sheet is not from one single point, but from a number of reflected points. This area, or zone, is termed as the Fresnel Zone, and can be viewed in Figure 2.2. From this zone, the two way path length from source to receiver is at its most $\lambda/4$ longer than the nominal path length. The intensity spread from points in the first Fresnel Zone then arrives less than a quarter period after the nominal arrival, thus, the energy interferes constructively. The shape and size of the Fresnel Zone is dependent on the position of the source and the receiver, the velocity, and the wave length [16] [18]. The area which effectively contributes to a reflection is sometimes referred to as the "effective" Fresnel Zone (Equation 2.13) where h is the vertical depth, and λ is the dominant wavelength.

$$R = r_f \approx \frac{1}{2}\sqrt{\frac{h\lambda}{2}} \tag{2.13}$$

For ice resonance this means that the Fresnel Zone represents the horizontal

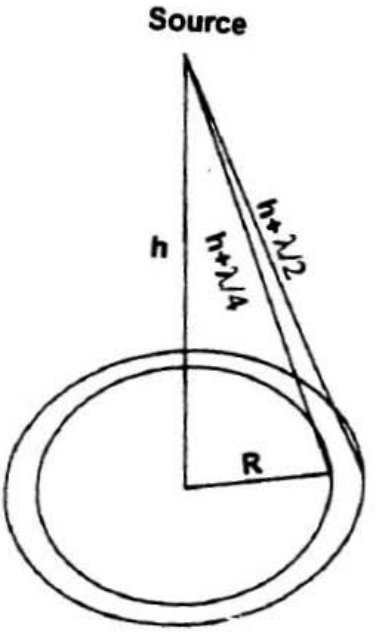

Figure 2.2: Fresnel Zone

circular footprint that the experiment will cover. However, in the case of determining the depth of ice from the first reflection time, the signal can only be as accurate as a 1/4 the minimum wavelength.

2.1.4 Standing Waves and Resonance

D'Alembert has shown that the solution of the wave equation consists of the superposition of two terms, which are the functions $f_1(ct+x)$ and $f_1(ct-x)$. Each function denotes a wave moving to the right or to the left. For example, an expression of a string displacement of $f_1(ct+x)$ (Equation 2.14).

$$y = Ae^{i(\omega t - kx)} \tag{2.14}$$

Where $k = 2\pi/\lambda$ is the wavenumber, and λ is the wavelength in meters. A sheet of ice can be seen as a string of length l with its ends rigidly tied vertically at the ice-air boundary and the ice-water boundary. The displacement y on the string at any point can therefore be expressed by Equation 2.15.

$$y = Ae^{i(\omega t - kx)} + Be^{i(\omega t + kx)} \tag{2.15}$$

Where A and B are complex constants to be determined from the boundary conditions at $x = 0$ and $x = l$. These boundary conditions for a clamped string are $y = 0$ at $x = 0$ and $x = l$ results in $A = -B$ from equation 2.15. This condition means, physically that a wave is reflected at each end with a 180° phase change. The result of $y = 0$ at $x = 0$ and $x = l$ for all times t $sin(kl) = 0$ where $kl = n\pi$ (n=1,2,3..) or $k = n\pi/l$, which as an angular frequency that becomes $\omega_n = n\pi c/l$. These frequencies are called *Natural Frequencies*.

The natural frequency of an ice sheet can be visualized as a string tied at both ends as explained in the previous example. The resultant equation for the natural frequency of an ice sheet is addressed in Equation 2.16 where l is the depth, and n is the mode integer. A graphical representation of Equation 2.16 can be seen in Figure 2.3.

$$f = \frac{\omega}{2\pi} = \frac{V_i}{2ln} \tag{2.16}$$

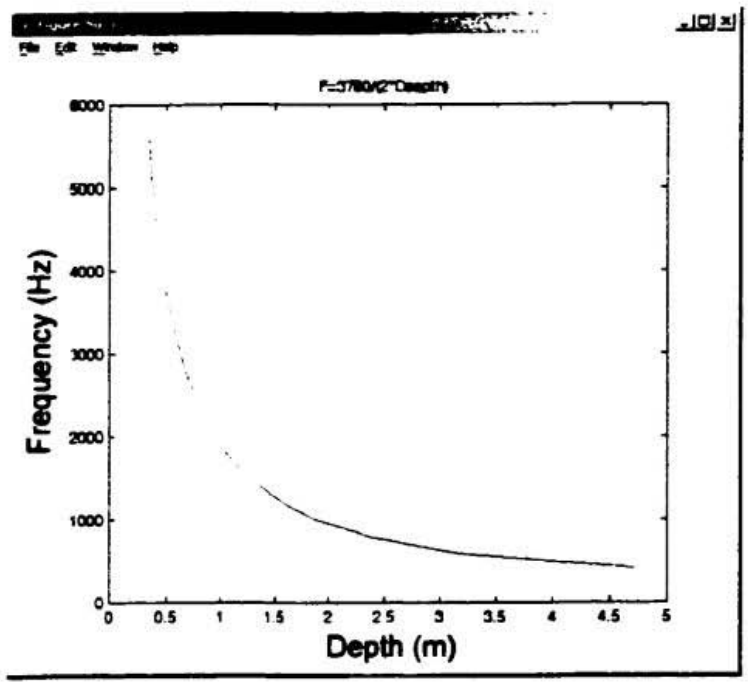

Figure 2.3: Frequency vs. Depth ($V_i = 3780m/s$)

2.2 Digital Signal Processing

Using the time and frequency evaluation techniques specified in Table 2.1, ice properties can be determined. For frequency analysis, the Fourier transform is used to take a time domain signal to its frequency domain. For determining the ice transfer function $h[n]$, discrete deconvolution is used. Finally, the techniques used for time analysis are FIR filter design, cross-correlation, geometric time difference, and minimum/maximum search. In the following sections, sampling theory, and the functions in table 2.1 will be discussed carefully.

Data	First Stage	Second Stage	Third Stage	Result
Digitized Signal and Low pass analog filter (8KHz)	Multi Pole Band Pass FIR Filter	Cross Correlation	1st and 2and Max Peak	p-wave velocity and ice depth
	Inverse Convolution	Impulse Response $H(j\omega)$	Dominant Frequency Search	Ice Depth
	FFT With Hamming Window	Dominant Frequency Search	—	Ice Depth

Table 2.1: Method of Digital Signal Analysis

2.2.1 Sampling and Resolution

When designing an analog (continuous or not computerized) to a digital (discretized or computerized) sampling system, care must be taken to ensure that the system has a sampling frequency that is adequate to prevent possible high frequency aliasing and that the system has the dynamic range to resolve the signal's amplitude variability. According to the Nyquist Sampling Theorem, if $x_c(t)$ is a bandlimited signal with $X_c(j\Omega) = 0$ ($X_c(j\Omega)$ is $x_c(t)'s$ frequency amplitude) for $|\Omega| \geq \Omega_N$ Then $x_c(t)$ is uniquely determined by its samples $x[n] = x_c(nT), n = 0, \pm 1, \pm 2, \ldots$ if $\Omega_s = \frac{2\pi}{T} \geq 2\Omega_N$. The frequency Ω_N is commonly known as the Nyquist Frequency which is the minimum sampling frequency that can be used without corrupting the sampled data. In practice, sampling rates above the Nyquist Frequency are used to allow

for non-ideal filtering. For example. Figure 2.4 shows a signal being represented at multiple levels of the sampling period. T. where $x[n] = x_c(nT)$ is less than twice the Nyquist Frequency. Because the sampling frequency is less than the Nyquist Frequency. a type of signal corruption called aliasing occurs where two frequencies can be represented by the same points.

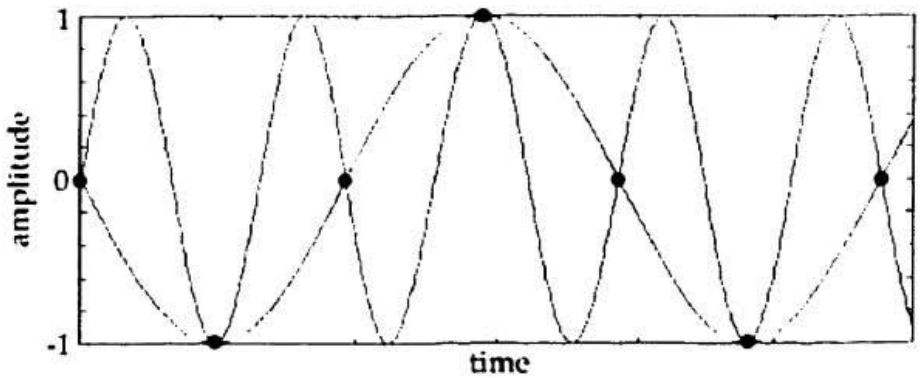

Figure 2.4: Aliasing: Two Frequencies Represented by the Same Samples

The bit resolution of a sampled signal dictates the amplitude the computer can resolve. The signal amplitude resolution of the "n" bit system would be as in Equation 2.17. For example. 8 bits will result in a resolution of 24 decibels (dB). whereas 12 bits represents 36 dB. and 16 bits represents 96 dB.

$$Resolution = 20log(2^n)dB \tag{2.17}$$

For example. a 12 bit system with a 0 to 5 volt range can resolve $2^{12} = 4096$ points or a voltage no smaller than $\frac{5}{4096} = 1.2mV$.

2.2.2 Fourier Transform

Equation 2.16 requires the determination of the lowest resonance frequency harmonic of an ice sheet to determine the thickenss. Hence. the time sampled vibration needs to be viewed in the frequency axis. The discrete Fourier Transform is used to transform

a time domain signal to the frequency domain representation. The transform is accomplished by calculating the sum of all the products of a function at point "n" with the cosine wave and sine wave at point "n" in reference to a specific frequency. All frequencies are set between 0 to 2π where 2π is equal to the sampling frequency. The results for each frequency are a real and imaginary values (Equation 2.18). The squared sum of the two values yields the magnitude of the specific frequencies.

$$X(e^{j\omega}) = \sum_{n=-\infty}^{\infty} x[n]e^{j\omega n} \tag{2.18}$$

However, Equation 2.18 is for continuous infinite signals where this experiment's sampling time of a discrete time. A sampled signal windowed at a finite interval contains undesirable high frequency artifacts at its sharp discontinuous ends. This phenomenon is called the Gibbs Effect. To reduce the Gibbs Effect, a windowing function can be multiplied onto the signal such as Hamming and Hanning type windows as illustrated in Figure 2.5. These windows slowly taper a signal's amplitude at each end to zero, thereby diminishing the end of each window's discontinuity causing a significant reduction in the Gibbs Effect. While all the windows listed effectively reduce the Gibbs Effect, the most commonly used is the Hamming window due to its consistently excellent results. The windowing addition to a discretised finite length sample can be seen in Equation 2.19.

$$X(e^{j\omega}) = \sum_{n=0}^{L} x[n]e^{j\omega n} \cdot w[n] \tag{2.19}$$

2.2.3 Digital Filtering

Once a signal is sampled, bandpass filtering can be conducted to further remove any unwanted frequency components such as transducer and electronic oscillations. There are two possible techniques in which filtering can be conducted. The first technique involves the application of a Fourier Transform, followed by the multiplication of the frequency based signal by a step function at the desired frequency. The final step involves the application of an inverse Fourier Transform. The second method requires the convolving of a signal with a bandlimited transfer function $h[n]$. Convolution is

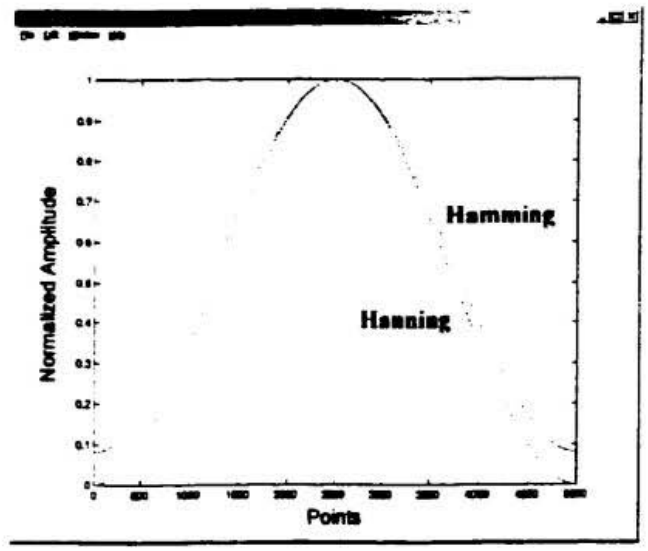

Figure 2.5: Hamming and Hanning Windows (5000 points)

shown in Equation 2.20 where x[n] is the input signal and y[n] is the output signal.

$$y[n] = \sum_{k=-\infty}^{\infty} x[k]h[n-k] = x[n] * h[n] \tag{2.20}$$

These two methods of signal manipulation are depicted in Figure 2.6. Although the transformation of a signal to a frequency domain is visually the simplest method of filtering, convolution is the most direct method. Convolution also requires the least calculations: therefore, for filtering, convolution will be used.

The two principle types of convolving filter designs are the Finite Impulse Response (FIR) filter and the Infinite Impulse Response (IIR) filter. FIR filters are based on the Fourier transform and windowing, where as IIR filters apply the impulse response of analog filters such as Butterworth and Elliptic filters. An essential feature of an FIR filter is that it contains the desirable property of constant group delay, therefore, for the experiments in this thesis, the FIR filter method will be used. Like the Fourier transform, FIR filters require windowing, w[n], to reduce unwanted corruption, and once again, the widely used Hamming window function will be used

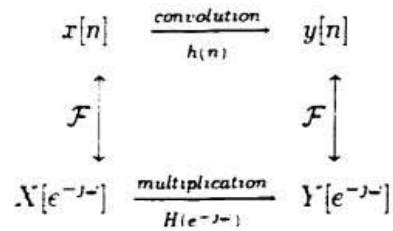

Figure 2.6: Convolution to Fourier Relationship

to reduce the Gibbs effect.

The generalized linear phase FIR filter is designed starting with the following equations. For a low pass filter, the boundary conditions are set as follows in equation 2.21.

$$H_{lp}(e^{j\omega}) = \begin{cases} e^{-j\omega M/2}, & |\omega| < \omega_c, \\ 0, & \omega_c < |\omega| \leq \pi. \end{cases} \tag{2.21}$$

Then from these boundary conditions, h[n] is determined using Equation 2.22.

$$h_{lp}[n] = \frac{1}{2\pi} \int_{-\omega_c}^{\omega_c} e^{-j\omega M/2} e^{j\omega n} \partial\omega = \frac{\sin[\omega_c(n - M/2)]}{\pi(n - M/2)} \tag{2.22}$$

Where ω_c is the cut off frequency and M is the number of points (poles). However, to reduce the Gibbs effect, a windowing function $w[n]$ is multiplied into the Equation 2.22 as in Equation 2.23.

$$h_{lp}[n] = \frac{\sin[\omega_c(n - M/2)]}{\pi(n - M/2)} w[n] \tag{2.23}$$

For a high pass FIR filter, the equations are as follows.

$$H_{hp}(e^{j\omega}) = \begin{cases} 0, & |\omega| < \omega_c, \\ e^{-j\omega M/2}, & \omega_c < |\omega| \leq \pi. \end{cases} \tag{2.24}$$

The corresponding impulse response, h[n], can be determined by evaluating the inverse Fourier Transform of $H_{lp}(e^{-j\omega})$ or observing that

$$H_{hp}(e^{j\omega}) = e^{-j\omega M/2} - H_{lp}(e^{j\omega}) \tag{2.25}$$

Where $H_{lp}(e^{j\omega})$ is seen in equation 2.22. so $h_{hp}[n]$ is:

$$h_{hp}[n] = \frac{\sin[\pi(n - M/2)]}{\pi(n - M/2)} - \frac{\sin[\omega_c(n - M/2)]}{\pi(n - M/2)}, \quad -\infty < n < \infty \tag{2.26}$$

The group delay of the high pass and low pass filter is defined in equation 2.27 where the function 'ARG' determines the phase of the function by taking the real and imaginary portions of $H(e^{j\omega})$ and calculating the angle between them. In the case of FIR filters, the group delay (grd) will be constant.

$$\tau(\omega) = grd[H(e^{j\omega})] = -\frac{d}{d\omega}\{arg[H(e^{j\omega})]\} \tag{2.27}$$

For example, when a low pass filter with a cut off frequency at $\pi/4$ is designed with 100 poles the resultant h[n] is a sinc function as seen in Figure 2.7 and the resultant group delay can be seen in Figure 2.8 as being delayed by 50 samples.

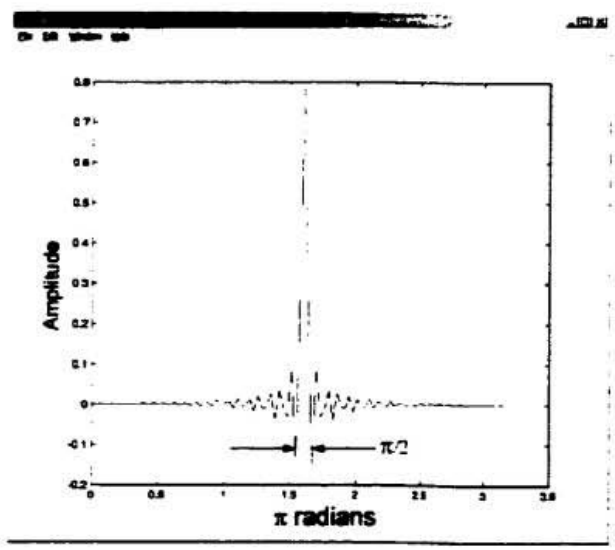

Figure 2.7: Low Pass Filter h[n] at $\frac{\pi}{4}$ Example

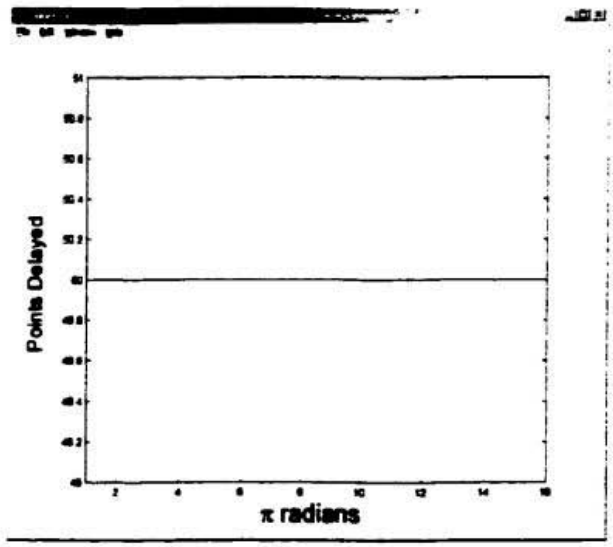

Figure 2.8: Low Pass Filter Group Delay of Figure 2.7 Example

2.2.4 Inverse Convolution

Another method for determining the characteristics of a system such as an ice sheet is to find the transfer function or $H(e^{j\omega})$. More clearly, the transfer function of a system is its frequency response over all frequencies. For an ice sheet, the most dominant frequency would be its depth resonance. Figure 2.6 shows the paths that can be taken to determine $H(e^{j\omega})$ from x[n] and y[n] where the simplest route is to take the Fourier transform of x[n] and y[n] then divide the two as seen in equation 2.28. For this experiment with ice, directly obtaining x[n] is not possible, but an approximation can be made by inserting instrumentation on or near the source of impact [18].

$$H(e^{j\omega}) = \frac{Y(e^{j\omega})}{X(e^{j\omega})} = \frac{\mathcal{F}(y[n])}{\mathcal{F}(x[n])} \tag{2.28}$$

2.2.5 Cross-correlation

Cross-correlation [20] is effective for comparing two waveforms for similarity. The advantage of cross-correlation is that it matches signal shapes regardless of the signal amplitude. For example, if two decaying sine waves of the same frequency and different starting amplitudes were cross-correlated together, the strongest correlation would be when the start of the first wave matched the start of the second wave. The formula for cross-correlation can be seen in Equation 2.29, where g and z are each signals of the same length. The resultant output length is 2*M-1 where M is the length of the original two functions.

$$\upsilon_{gz}(\tau) \equiv \int_{-\infty}^{\infty} g(t)z(t+\tau)\partial t \tag{2.29}$$

2.3 Impact Bandwidth

For a sheet of ice to "ring" at its resonance frequency, an impulse must be added to the ice that contains the frequency component of the resonance. Such an impulse can come from a hammer, a bullet or any type of similar impactor. For example, for a frequency bandwidth from 0 KHz to 10 KHz, the type of impulse required can be seen by conducting the inverse Fourier transform as seen in equation 2.30. The result is the sinc function as seen in equation 2.31, therefore, for a hammer impulse of 10 KHz to be effective, an impulse the shape of a 10 KHz sinc function is required though other linear time invariant functions can closely match this requirement. Note that in Equation 2.31 $\sqcap$ represents a band limited function with a cut off frequency at f.

$$x[n] = \frac{1}{2\pi}\int_{2\pi} X(e^{j\omega})e^{j\omega n}\partial\omega \tag{2.30}$$

$$\mathcal{F}^{-1}(\sqcap(f)) = sinc(\pi f) \tag{2.31}$$

However, a sinc function is a non causal-wave, and there is no impactor capable of creating such an impulse. A more likely impulse would be a $-\pi/2$ shifted sinc (Figure 2.9). But to demonstrate that this discontinuous function still contains the required bandwidth, the Fourier transform of this function [21] are illustrated in

Figure 2.10.

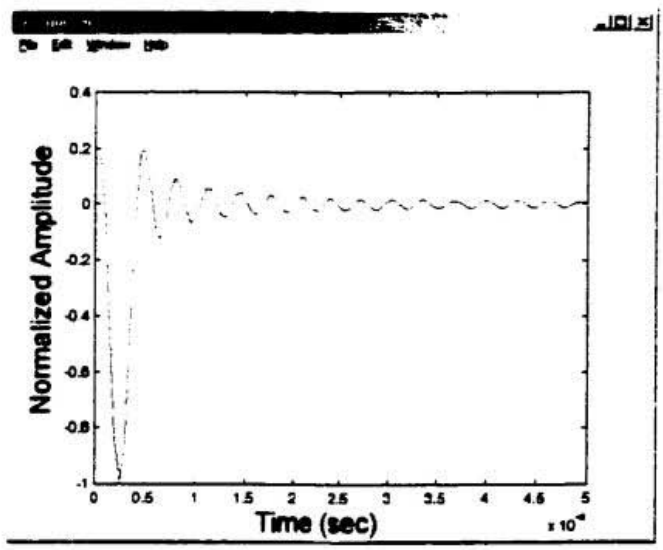

Figure 2.9: 10 KHz Impact Example

2.4 Feasibility

Feasibility calculations to determine the system specifications are made from the existing theory. To start, from Equation 2.16 and Figure 2.3, the acoustical range between 0.2 and 10 KHz corresponds to a typical ice depth of 0.2 m and 10 m of ice. With a frequency range of 10 KHz, the Nyquist frequency is 20 KHz and then ten times the sampling frequency to ensure that aliasing will not be present with unideal filters, puts the minimum computer sampling frequency at 200 KHz.

Reflection energy loss is calculated from Equation 2.9 with the H_2O and air characteristics in table 2.2. The results are summarized in table 2.3 below.

The losses in table 2.3 indicate that poor air coupling of a transducer and actuator to an ice surface must be eliminated for this experiment to be viable. The other indication is the reflection losses at the ice-water boundary are -8.0 dB per reflection which indicates that if the mechanical waves reflect only from one point source (worst

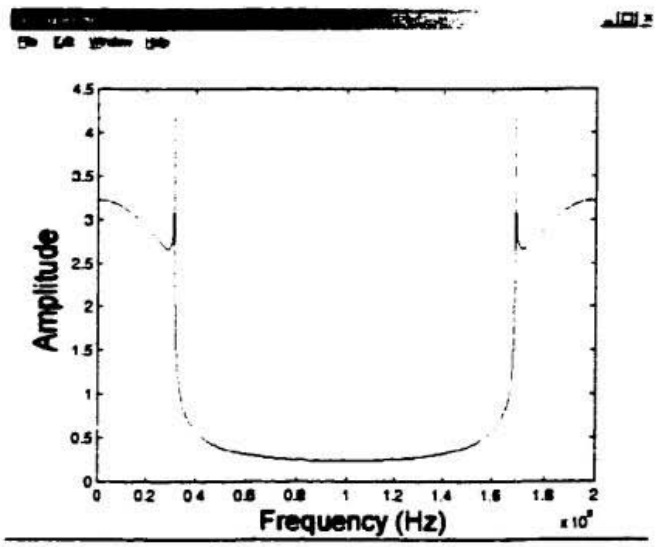

Figure 2.10: Fourier Transform of the 10 KHz Impact Example

Substance	Velocity (m/s)	Density (Kg/m^3)	$V * \rho$
Air	328	1.26	413
Water	1435	1000	$1435 \cdot 10^3$
Ice (fresh -5C)	3780	917	$3465 \cdot 10^3$
Ice (salt 5% -5C)	3100	813	$2520 \cdot 10^3$

Table 2.2: H_2O Characteristics

case scenario), the resolvable reflections with an 8 bit system (24 db) are 3 reflections and with a 12 bit system (36 dB) 4 to 5 reflections. For these experiments, a 12 to 16 bit system will be adequate as long as the background noise is low.

Transmission/Reflection	Loss	Loss in dB
Air-ice (ice-air)	0.00067	-32
Ice-water reflection	0.16	-8.0
Ice-Water transmission	0.84	-0.7

Table 2.3: Ice-Air, Ice-Water Refection and Transmission

2.5 Conclusion

The theoretical background indicates that the ice resonance method is a viable methodology to determine ice depths. The resolving limits are with-in computer capabilities and electronic sensitivity as 12 bit digital resolution is an industry sensor instrumentation standard and 1000 MHz computer sampling rates are very common. Additionally, impacting and sensing bandwidths are realistic values to be developed. This stage of research indicates a "go-ahead" with further development of electronic hardware and computer software for the specifications determined.

Chapter 3

Design Implementation

Measuring ice resonance requires a very particular system. However, with proper selection of parts and accurate calibration a very close approximation can be made. Interpreting this system requires the implementation of wide bandwidth actuators, sensitive transducers, and a computerized system. Within the computerized system there must also be resolution available to resolve the signal's dynamic range as well as software tools to evaluate the data.

The design process started as a high level system diagram (Figure 3.1), where each part is addressed as an individual problem which must be solved. Once the sub-components were completed, they were integrated back into the original plan, the system as a whole was debugged and then the system design was continued to completion.

Choosing the correct components was an iterative process which began with a collection of specifications requiring each component to have a basis that it could be built from. These specifications were determined by manipulation of the calculations in Chapter 2 and a review of the previously published materials, found in Chapter 1, and placed in Table 3.1. The information in the table sets the boundary conditions which were used to design the setup for this experiment.

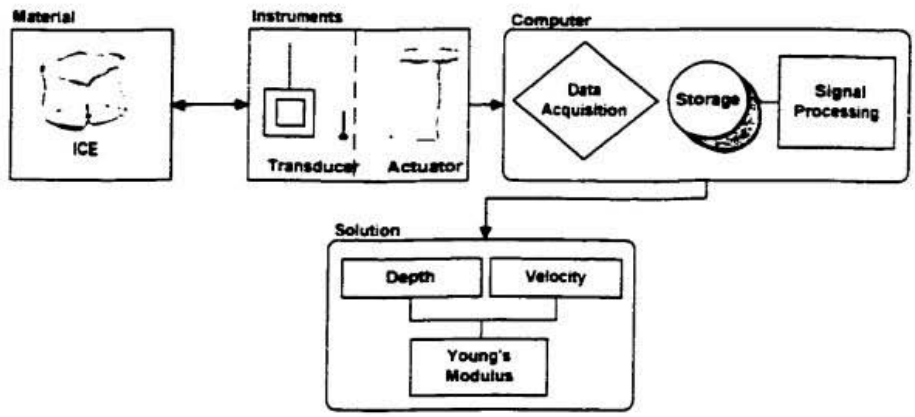

Figure 3.1: High Level Design

3.1 Transducer

3.1.1 Electronics

As specified. the desired sensor is a biaxial accelerometer with the resolving capability of 10 KHz that is also capable of retaining a high vibrational sensitivity. Some of the products considered were: B& K. Entranm. Analog Devices. and generic piezo electric sensors. The final choice began with the most cost effective product and proceeded by conducting a series of experiments. which tested the efficiency of the proposed products.

The experiments started with a generic 3.KHz piezo electric device. These devices commercially sold have a natural resonance frequency of 2.5KHz to 3 KHz. but as seen in Figure 2.3. resonance at this frequency range corresponds to an ice depth of approximately 1 m which is undesirable. Additionally. after conducting some short experiments on 0.12 m lab ice at -3C. the ceramic was found to contract and crack which rendered the accelerometer non-functional.

The next device evaluated was the Analog Devices. ADXL105. surface mount chip. (Figure 3.2. Appendix D). This device is a capacitive accelerometer suspended in silicon. it also includes a calibration and frequency response graph (Figure 3.3). According to the manufacturer's specifications. the ADXL105 has a flat response

Part	Spec	Requirement
Transducer	Temperature Range	-40 — 0 C
	Vibration Sensitivity	250mv/g
	Axis	Biaxial (x+z)
	Frequency Response	200Hz —10 KHz
	Power	Low (miliwatts)
	Mass	$\approx 0g$ ref: ice sheet
	Coupling to Ice	Transparent
Actuator	Impact Type	Impulse
Actuator Instrumentation	Frequency	10 Khz
	Mass	$\approx 0g$ ref: actuator mass
	Sensitivity	Impact
	Temperature	-40 — 0 C
Data Acquisition Device	Resolution	$> 30dB$ (12bits)
	Sampling Frequency	>200Khz/ch
	Number of Channels	6
Software Tools	Data Acquisition	LabView
	Computation	Matlab
	Storage	>10Gb

Table 3.1: Specifications

that is close to the regions of interest for this experiment. It is sensitive up to 2 mg/volt of vibration, and was rated to function in temperatures -40 C.

As the ADXL105 was able to accommodate the required specifications it was the used for this investigation. However, the chip required a circuit which needed to be built independently.(Figure 3.4). Additional circuitry not shown in Figure 3.4 is the support for the device's power needs, a double pole low pass filter (8 KHz), and an output low impedance amplifier (needed for noise suppression on long cables). As the ADXL105 is only single axial, two chips were placed perpendicular to each other in the same packaging to accommodate x and z components. An important aside pertaining to the design is the analog low pass frequency filtering. The two reasons for using low pass filtering are to reduce the signal to noise ratio and to prevent high frequency aliasing.

OUTLINE DIMENTIONS OF THE ADXL105

Dimensions shown in inches and (mm).

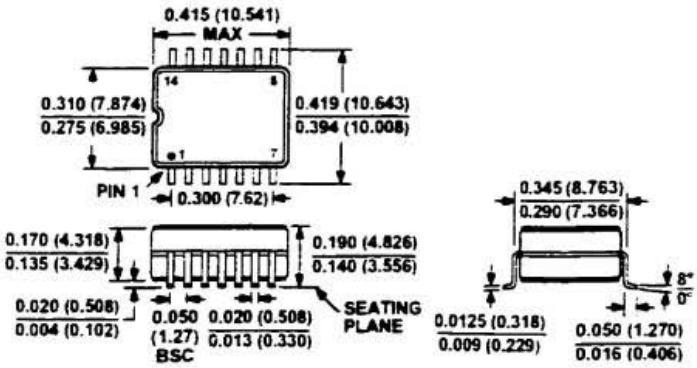

Figure 3.2: ADXL105 Dimensions

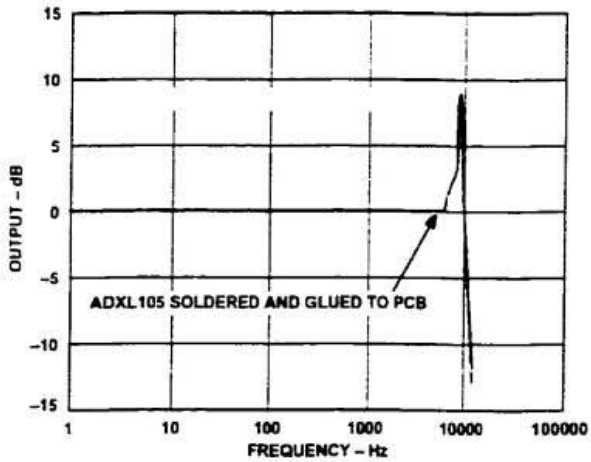

Figure 3.3: ADXL105 Calibration

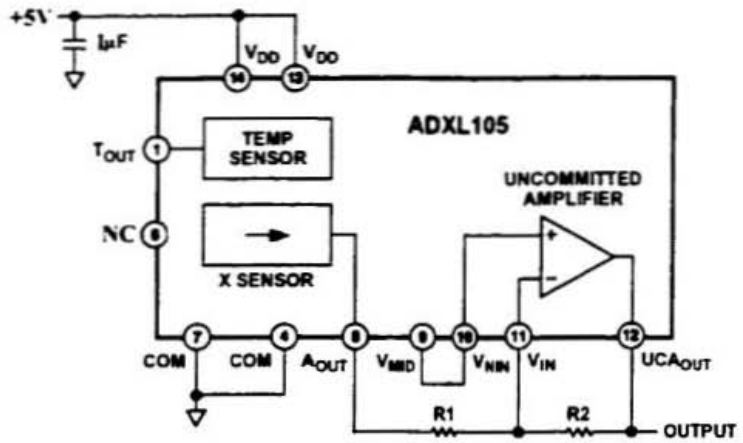

Figure 3.4: Basic ADXL105 Electronics

3.1.2 Packaging

A sensor, when used properly, should be unnoticed by the environment it senses, have a minimum effect on the ice, and the packaging should be as minute as possible, yet it should still contain the necessary electronics. As specified in Figure 3.1, the device must be able to function (i.e. not crack or severely contract) in extremely cold conditions, avoid resonance in the desired frequency range, and have nearly transparent coupling with ice and electronics circuit boards (i.e. very hard material).

Resonance is present in all materials built. Nevertheless apparatus can be designed to reduce the resonance produced as much as possible and still exclude it from the frequency of interest. In this experiment, resonance should be above the 10 KHz range. This is accomplished through selecting a very rigid material and keeping its dimensions as small as possible.

The current options available for such analysis are off-the-shelf small plastic boxes, epoxy resin enclosures, custom plexiglass and aluminum boxes. Of these four options the off-the-shelf boxes are the softest, having very thin edges making them unsuitable to be considered any further. Epoxy resin hardens, therefore post construction alterations or electrical malfunctions would be impossible to repair. Remaining are

the plexiglass and the aluminum. Both are rigid and relatively inexpensive, however each had unique features not present in the other appartus.

Aluminum is a good conductor and according to Maxwell's equation 1 (Gauss' law), Equation 3.1, the electrical field inside a conducting surface is zero. For the transducer, this would mean that all external electrical noise could be suppressed, hence, increasing the signal to noise ratio.

$$\oint \vec{E} \partial A = \frac{q}{\varepsilon_o} \tag{3.1}$$

The plexiglass, however, is transparent. Physically this feature is not important, but in the field, simple maintenance is paramount which makes transparency a desirable option. Checking for water leakage, seal problems, broken wires, and chip failures can be quickly evaluated and corrected with a clear enclosure. Therefore, from this simple evaluation of available materials the best choice would be the plexiglass. The plexiglass box was designed to be as small as possible while retaining its strength and ability to contain the electronics. The device built is illustrated in Figure 3.5.

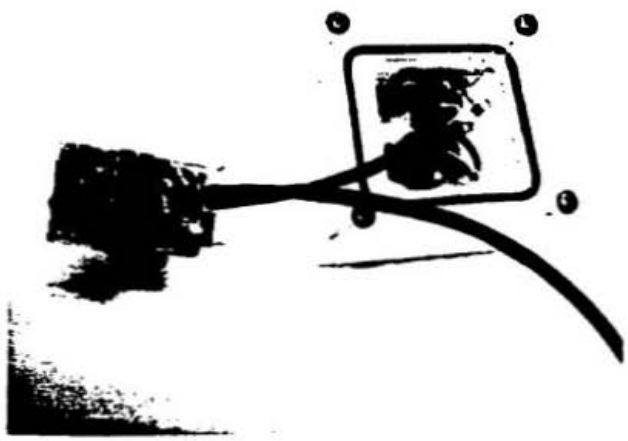

Figure 3.5: Packaging

3.1.3 Calibration

Calibrations consisted of three steps:

1. Verification of electrical characteristics (i.e. no electrical resonance and correct frequency response.
2. Verification of ADXL105 frequency response and sensitivity.
3. Entire packaged system frequency response.

Electrical Characteristics

To ensure that the electrical circuitry functioned as designed. using linear amplification and an 8 KHz low pass filter. the subsequent experiment was conducted. A frequency generator was connected to the output posts of an unconnected ADXL105 to simulate the output of this chip. The frequency generator's frequency was then increased from 0.010 KHz to 20 KHz and the voltages were recorded at the sensor's plug. The result was a flat response. With an unmeasurable signal to noise ratio. This result indicated that no electrical alterations were needed.

ADXL105 Characteristics

The supplied graph for the ADXL105 is shown in Figure 3.3. This figure shows that the device has a flat frequency sensitivity up to 6 KHz and from this point it has a linear gain from 0 dB to 3 dB at 8 KHz. Note that the calibration of this device is dependant on the device being securely mounted to the circuit board to which it is wired.

Physical Analysis

Following the prementioned trial. the completed transducer was placed in a linear calibrator. B& K 4291. However. the calibrator is only "in calibration" at 0.078 KHz and any other frequency recorded is in reference to 0.078 KHz. Although the frequency can be altered. upon alteration the device does not stay in calibration. An example of this occurred when a single ADXL105 was epoxied onto a small screw and then placed on the B& K calibrator. The frequency was altered over a range

between 0.010 and 10 KHz. These observations meant the B& K calibrator would resonate (which was distinctly heard and seen as the device would enter oscillation) over a series of frequencies.

Although a frequency sweep is not particularly useful, this calibrator is useful for two reasons. The first is to find the transducer sensitivity at 0.078 KHz and to make the appropriate amplifier alterations; the second is to insure that there is a baseline sensitivity for the device that is needed for signal power calculations.

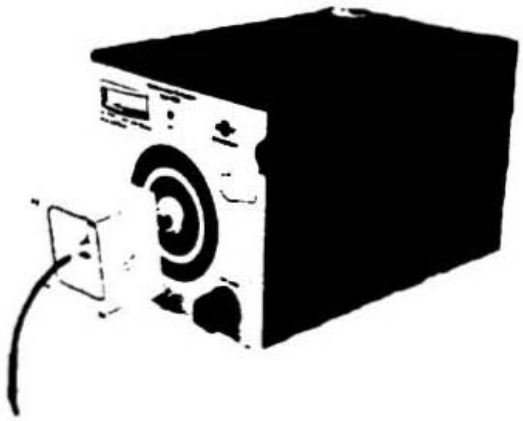

Figure 3.6: B& K Calibrator with Transducer

The last stage in calibration was to determine the package resonance from an impulse. The test was completed by hanging the transducer by its electrical wires (the weight of the wires being negligible) and tapping the transducer with a small metal ball-peen hammer. The signal was then recorded and a 4096 point Fourier Transform was conducted using the data (Figure 3.8). The points of interest are the resonance points and the decay time. First, the series of resonances at 6, 7, 11, 13.5, 14.5, 15 and 17.5 KHz and particularly, the peaks at 6, 7 and 17.5 KHz were very strong. The resonance at 6 KHz is of most interest because it limits the frequency resolvability of the transducers to a bandwidth of 6 KHz, which corresponds to an ice depth of no less than 0.32 m. Additionally, the decay time of the transducer's resonance is of the order of 15 ms for a 3 dB change in power. When the device is

frozen onto a large ice sheet, the decaying signal was to the order of 2.5 m/s (500 samples). Figure 3.9.

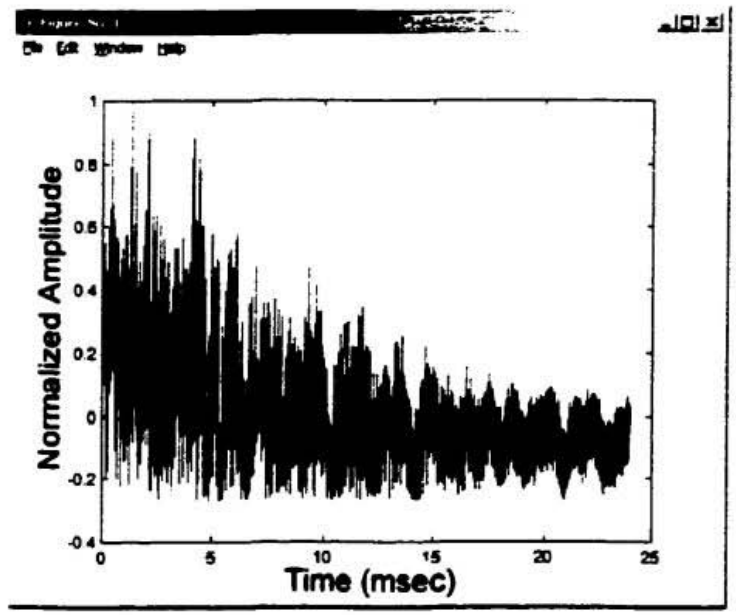

Figure 3.7: Hammer Impulse on Sensor (Time)

In terms of this area of research, it is important to distinguish if these resonances can be removed or altered. Options for such research within the scope of this project are to either redesign the transducer package, which due to the size of the electronics is not reasonable, or to determine if the proposed experiments can be conducted regardless of the resonance using digital and analog filtering.

If the receiving signals in an experiment are large enough in amplitude to overcome resonance amplitudes without saturating the sensor, the resonance corruption will not effect the experiment. Additionally, the received signal can be digitally filtered to remove all corrupting information and a time signature can then be obtained.

The final information to be considered is the device's signal to noise ratio. In laboratory conditions, the noise created by the device is 24 mV corresponding a signal to noise power of 26 dB (Figure 3.9).

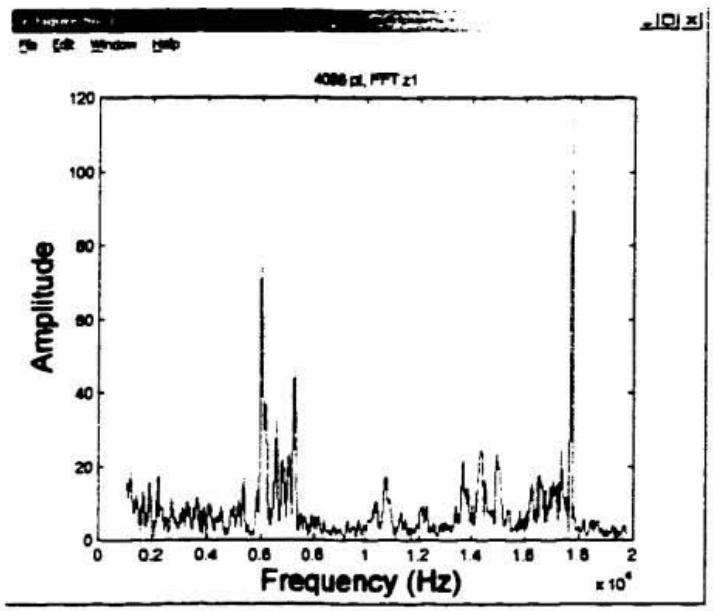

Figure 3.8: Hammer Impulse on Sensor (FFT, 4096 points)

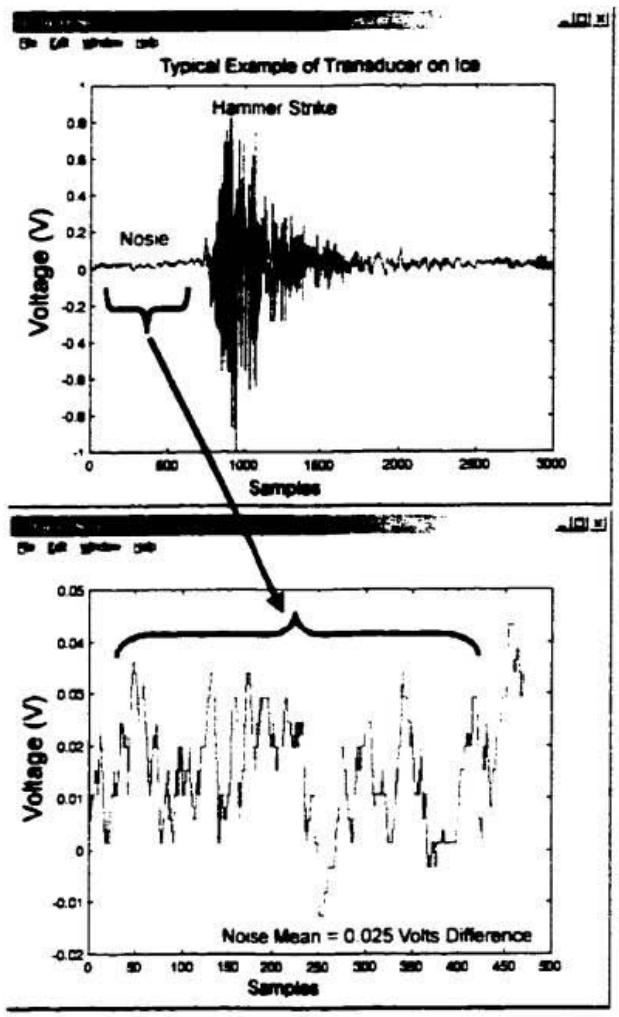

Figure 3.9: Sensor Noise

3.2 Actuator

The actuator is needed to apply an impulse to "ring" the ice. Other options such as a "chirp" device could have been used. however. the impulse was used because of four constraints. Power consumption. complexity. [16]. and availability are all commonly considered when conducting seismic research. A perfect impulse is impossible to realize. but the desired impulse needs only to contain the harmonics of a 10 KHz bandwidth. This type of impulse is a realizable impact. Upon investigation of impact devices to use. a review of the geophysicist's tools was checked [16]. [18] as seen in Section 1.2.3. As previously mentioned. seismologists use tools such as dynamite. jackhammers. large weights (1/2 Tonns), and sledge hammers. In scaling these devices to the size of this experiment. the device emerged as being a simple hammer. The question which remained was the type of hammer to be used.

The options available were a small metal ball-peen hammer. a plastic-headed hammer. or a heavier rubber-headed hammer. The decision was made after evaluating hardness. The less stiff the substance. the lower the bandwidth of the impulse delivered to the ice. Therefore. the hardest material. the metal ball-peen hammer was used. Using this hammer created a risk of cracking the ice. but it is assumed that cracking does not affect resonance measurements. nevertheless attention will be paid when observing timing information.

Figure 3.10: Impact Hammer

3.2.1 Electronics

The desired goal is to instrument the hammer so that:

- Timing information can be collected (ie. computer data acquisition triggering)
- Power spectrum, and hence an impulse response, $h(t)$, of the ice can be determined.

To complete these two tasks, an impact sensor was added to the head of the hammer (Figure 3.10). The device's characteristics were chosen as specified in table 3.1. Such a device was the B& K type 8200 impact sensor and its associated B& K amplifier (Figure 3.11. The frequency response of the sensor supplied by B& K was flat between 0.01 and 8 KHz.

Figure 3.11: Hammer Setup

3.2.2 Calibration

An advantage of the B& K impact sensor is its own supplied calibration. Unfortunately, the impact device was discovered to saturate upon impact with hard surfaces.

This is undesirable and nullifies the detection of an impulse response portion in this experiment. Additionally, timing information is *fuzzy*, however, with the use of two transducers instead of one, accurate timing information was determined.

3.3 Data Acquisition

As specified in Table 3.1, the system required must sample the data at least twice with the bandwidth of interest (aliasing prevention) and be at least 5 μ seconds per sample, for a timing error of less than 1 percent with a signal amplitude resolution of greater than 12 bits (or 30 dB - see degradation of acoustical signals). Also, the system must be able to store multiple experiments and Megabytes of data.

The data acquisition device chosen was a pentium class computer with a $National Instruments^{TM}$ 12 bit data acquisition internal card. The card has 8 differential channels at 12 bits multiplexed over 1.2 Mega samples per second. Since this experiment only calls for five high speed channels and one low speed channel ($Hammer, Transducer1_x, Transducer1_z, Transducer2_x, Transducer2_z, temperature$), a sampling frequency of 200 KHz is possible.

3.4 Data Processing Tools

Data processing contains two levels of analysis. The first is conducted in the field and the second is required for post processing and precision analysis. In the field, before experimentation is begun, it is essential to conduct high speed data sampling, parsing, calibrating, system self test, and storage. This process was written using National Instruments LabView 5.x software and a picture of the program written can be seen in Figure 3.12.

Acquisition process started with a system self test of the power supply, transducer functionality, and a sample of outside temperature. The program then waits until a rising signal edge trigger, the hammer, before acquiring 70.000 points of data using 5 channels at a rate of 200.000 samples/second. Once the data is acquired, all data is displayed through graphs depicting the time and frequency domain (5000 pt FFT). Finally, the data is then written to a Matlab readable data file for later analysis.

Part two of the data processing is, as mentioned, the post-processing using Matlab 5.x. The functions of interest are filtering, Fourier Transforms, cross-correlations, and convolution. An additional feature of Matlab is its "export to C++" option which allows for later realization of the concept in software.

3.5 Cold Temperatures, Humidity, and Enclosures

Cold weather dynamics of electronics and computer equipment is a very important factor especially with the type of equipment being moved in and out of cold temperatures. Therefore a careful evaluation has been dedicated to ensuring temperature tolerance. The identified cold weather considerations are:

- Computer health
- Transducer water proofing, and reaction to cold temperatures
- Actuators functioning in cold temperatures
- Cabling and Plugs

A PC computer packaging is obviously not designed to be taken outdoors or in wet snowy conditions. To avoid all problems involved with precipitation, frost and cold, a *hot box* to contain the computer, monitor, UPS, and junction boxes was built. The keyboard and mouse had to be external to the box. The mouse was an optical mouse with no moving parts to freeze. The keyboard was tested in a -20 C laboratory cold room for functionality. The box was made from aluminum sheet metal with a plexiglass window so that the monitor could be viewed (Figure 3.13). The interior of the box was insulated with 0.04 m of foam where it was then lined with a heat blanket.

The transducer's plexiglass lid and wire exit holes were sealed using silicon. Preliminary laboratory-induced cold temperature experiments were run on the box by placing the box in a -20 C room for 24 hours. The sensor was then checked for physical deformations or cracks and given a functionality test on the B& K calibrator (a test for $\pm$ 1 g). The actuator was immediately brought into a +20 C room.

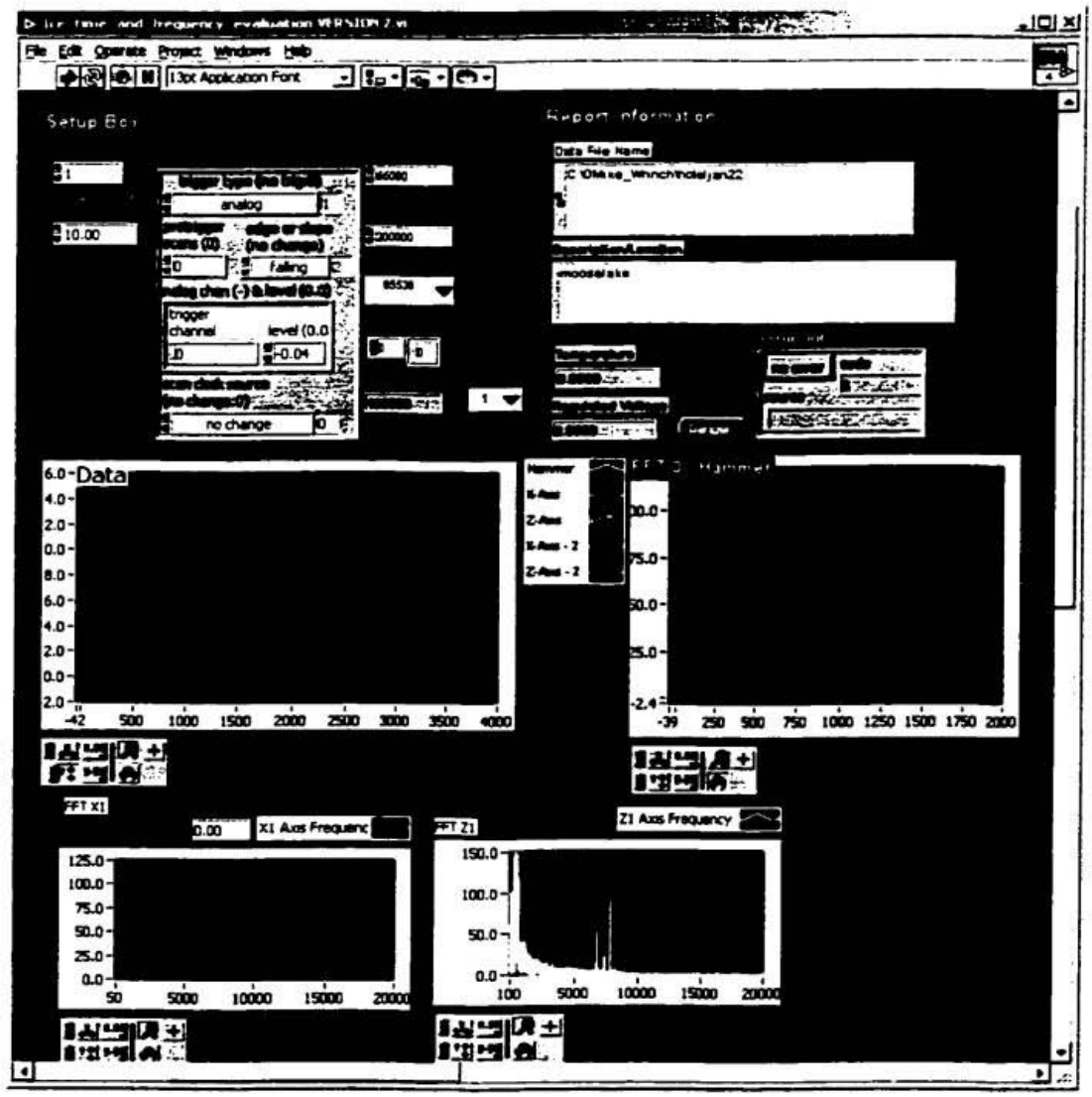

Figure 3.12: Data Acquisition Program

Figure 3.13: The Computer Box

The functionality test was repeated three times. The device showed no noticeable deformations or signal degradation.

Finally, the actuator and its amplifier were tested similarly in laboratory induced cold environments. The two devices were again checked for functionality by placing the amplifier and the hammer in a -20 C room for 24 hours, where the cables were checked for brittleness and a data triggering experiment was run. The test was repeated three times with no observed change in performance.

3.6 Power System

The electronics for this experiment required a 20 volt DC supply for the transducers and a 110 volt 400 watt AC supply for the heating box, monitor, and computer. This was achieved using a standard Honda generator in series with 300 feet of electrical wire, and an UPS (uninterruptable power supply) to remove dirty electrical noise from the generator.

3.7 Cabling

All electronics cabling was either double shielded cold temperature rated (transducers - power and signal). 50Ω co-axial cable (actuator) or standard outdoor 30 Amperes high current wire (computer and heat blanket)

3.8 Experimental Integration

The physical setup of the design of the experiment can be seen in Figure: 3.14. This design is a micro-version of a larger scale seismic system. additionally. two transducers are used instead of one for timing accuracy.

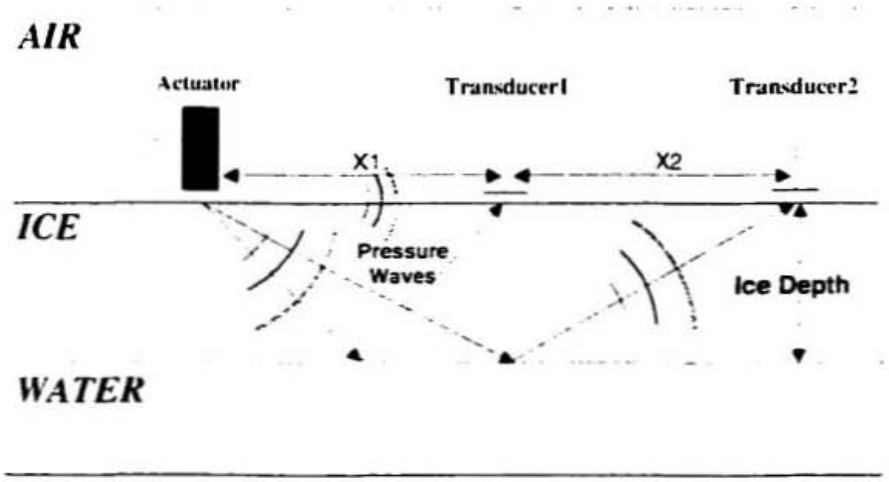

Figure 3.14: Experimental Design

3.9 Conclusion

This experimental setup has achieved a large portion of the minimum requirements. Critical successes are the sensor bandwidths and multi-channel. high frequency sampling. All other requirements are exceeded or are close to the criterion. Some inferior

components of the design include the impact senor saturation and signal to noise ratio of the transducers. Though preliminary experiments meet the specifications, the ability to resolve ice resonance can only be proven on actual ice sheets.

Chapter 4

Simulation

Before processing actual ice data, simulation can lead to insight for predicting if calculation processes will or will not reveal the desired result. Where the objective is to take arrival data from two transducers and calculate ice characteristics, such as velocity, and then from the resonance, calculate depth, several signal processing techniques will be reviewed and refined. The signal processing techniques experimented with are digital filtering (FIR), fast fourier transform, cross-correlation, and simple point to point matching.

The construction of the simulator was made in the Matlab environment where the data used to construct the simulator is a collection of information already known about the experiment and ice characteristics. Abnormalities of the transducer and computer equipment such as resonances, noise platform and quantization were reviewed and added. In the following sections, the construction, analysis and results will be reviewed in more detail.

4.1 Construction

Construction of the simulator consisted of three parts, the first being the theoretical signal arriving from the impulse, the second part is the corruption created by the transducer and computer, and the third is adding all the parts of the signal together to create a complete theoretical signal.

4.1.1 Signal Impulse

The arriving signal, the portion of the signal to be extracted from the corrupted signal, consists of four parts. The first is the original signal construction, the second is first arrival from the surface wave, the third is the reflection from the ice-water boundary, and the fourth is the decay of the resonance between the ice-water — ice-air boundary. Important considerations are the s-wave (shear) and p-wave (compression) arrival times. However as the s-wave travels approximately 1700 m/s and the p-wave travels at approximately 3780 m/s [5], hence the s-wave is only 44% the speed of the p-wave. Therefore for this simulator, the s-wave will not be considered.

During some initial experiments on simple ice sheets in a lab setting, typical wave-forms were recorded as seen in the example in Figure 4.1 and upon zooming into the arrival wave form, the first wave has a period of 0.6 msec or 1.7 KHz with smaller cycles of 0.2 msec indicating 5 KHz component. To try to recreate a wide bandwidth impulse of 5 KHz, a $1/4\pi$ shifted sinc function is used as an impulse to represent the time domain bandwidth of a 5 KHz impact shown in Figure 4.2.

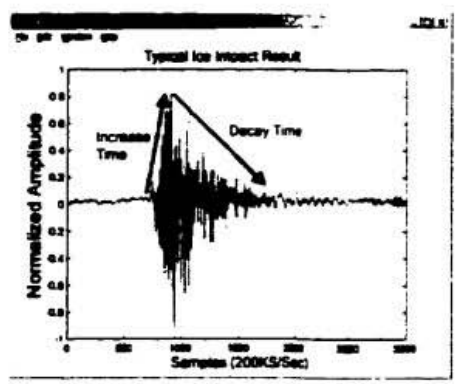

Figure 4.1: Typical Decay Time Example

Similarly, after the first arrival from the surface wave the first reflection arrives. The time of the first reflection is the geometrical difference between the surface and the direct reflection multiplied by the p-wave velocity as mathematically described using simple geometry as seen in equation 4.1. This wave will be a decayed version of the first sinc pulse of 70% as determined by Langleben in [22].

$$\Delta t V_p = 2\sqrt{(\frac{X_1}{2})^2 + D_{ice}^2} \tag{4.1}$$

Where X_1 is the distance between the hammer impact and the the first transducer and D_{ice} is the vertical depth of the ice sheet.

The next measurement to calculate is the resonance of the compression wave.

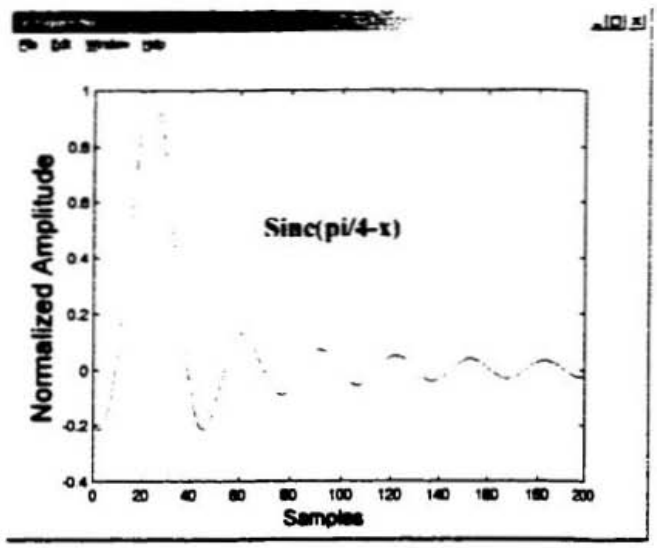

Figure 4.2: $Sinc(\pi/4 - x)$ at 200Ks/sec for 5KHz bandwidth

Resonance is explained in Chapter 2 however, in summary, the resonance is dependant on sound velocity and depth of the ice: $f_{resonance} = \frac{V_{ice}}{2 \times D_{ice}}$.

4.1.2 Sensors and Noise

During the calibration of the sensors (Figure 3.9), the white noise produced by a transducer is 0.025 Volts peak difference (-23 dB). Hence the white noise signal added to the simulator is a randomly generated signal of amplitude 0.025 volts. Additionally, the sensor has a series of resonances. The four most dominant resonance peaks as can be seen in Figure 3.8. These peaks were added to the signal frequencies of: 6000, 7000, 14500 and 17500 having normalized amplitudes of: 0.8, 0.6, 0.25, and 1 respectively.

4.1.3 Signal Decay

Figure 4.1 is a typical impact on an ice surface where the sensor measurement has a growth time and a decay time. For this particular envelope, the normal distribution

was used as an assumption for the envelope using equation 4.2. The rise time and decay time were once again taken from this graph as 2 msec for the rise time and 5 msec for the decay time. Note that from the design procedure, the sampling frequency to be used for all experiments is 200Ks/sec. Hence all data created is in reference to this sampling rate.

$$Envelope\_shape = \exp(\frac{-t}{\tau}) \tag{4.2}$$

Attribute	Type	Value
Noise	White	0.001
	6KHz	0.8
	7KHz	0.6
	14.5KHz	0.25
	17.5KHz	1
	18kHz	1
Noise Envelope	After first wave	0.001 sec
	Decay from max	0.001 sec
First Wave	Frequency	1.7 and 5KHz
	Amplitude	1

Table 4.1: Simulation Information

In the table 4.1 is a summary of the characteristics of the simulator. In addition, in Figure 4.3 is a picture of the signal in the time domain.

4.2 Simulation Evaluation

The simulator effectiveness can be best demonstrated by running an example evaluation of an ice sheet. For this example, the variables are as follows in Table 4.2 where typical ice characteristics were chosen such as 0.7 m ice, 200 KHz sampling rate and, 0.5 cm transducer separation. The evaluation process starts with a frequency analysis using a fast fourier transform, then time analysis by first filtering then running a cross-correlation and wavelet analysis.

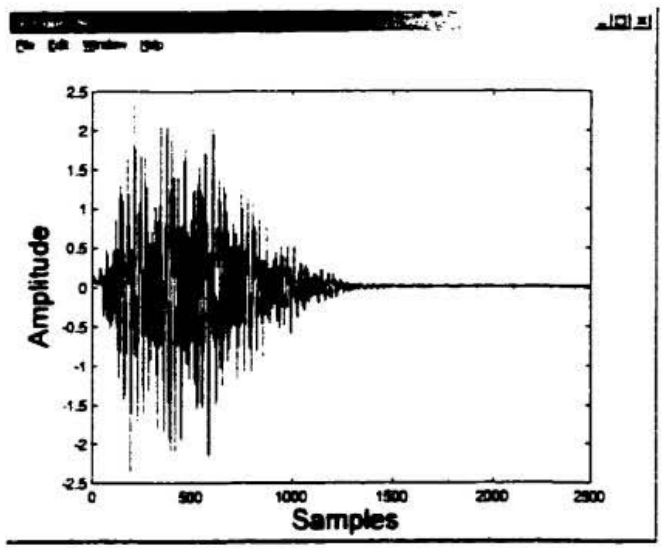

Figure 4.3: Simulated Signal

4.2.1 Frequency Analysis (FFT)

Frequency analysis is the heart of this experiment where a correlation is to be made with ice depth. First one must convert the data from the time domain to frequency domain using the Fourier Transform as seen in Equation 2.18. A Hamming window was used to reduce the Gibbs Phenomenon. Although other windows such as Blackman and Hanning would also work, the Hamming window was used. [23]

A 65,000 point Fast Fourier Transform was made for a frequency resolution of 3 Hz/point (200,000/65,000 = 3). However, because the actual signal energy is contained in under 2000 points of the 65,000 taken, the noise power overpowered any information about the transducer and ice signature. The only methods for overcoming this boundary is to reduce the window of signal in the Fourier Transform. Reducing the window size increases the Hz/Point, increasing the accuracy of the evaluation. For example, if a 4096 point Fourier Transform is performed on the data, the frequency resolution will be: $200,000/4096 = 49Hz/sample$ which is a depth error of 2% at 0.5 m. Incidentally, the 4096 point Fourier transform was the highest value that could be transformed before the desired signal was absorbed into

Characteristic	Attribute	Value
Ice		
	D_1	0.7 m
	V_1	3750 m/s
Computer		
	$f_{sampling}$	200 KHz
	$n_{sampled}$	66000 points
Transducer and Hammer		
	$T_1 - H$	0.5 m
	$T_1 - T_2$	0.5 m

Table 4.2: Simulation Example Data

the random noise platform, shown in Figure 4.4. Further clarification of the signal in time domain through filtering can be seen in the next section.

4.2.2 Digital Filtering (FIR)

Low Pass Filter

As the actual sensors contain only single pole 8.0 KHz filters, some unwanted noise can pass through the sensors' filter, and the electronics and cabling can cause noise. Further digital filtering will reduce the sensor noise. Similarly for the simulator, a multi-pole FIR filter can be used to reduce unwanted noise further and as the sensors are only calibrated until 8.0 KHz, a low pass filter will be a benefit. The reason for implementing a FIR filter instead of other filters like IIR Butterworth or Chebyshev filters is to achieve a constant group delay and linear phase shift. For more information on filtering definitions, see Theoretical Background Chapter 2. For this simulation, a 500 pole filter at a cut off of 7.0 KHz is used to remove all noise.

High Pass Filter

As the design of the sensor should be bandlimited between 0.190 and 7.0 KHz, a high pass filter was implemented to remove excess noise. Similar to the Low pass filter, a 500 pole FIR high pass filter will be implemented with a cut off frequency at 0.190 KHz. The resultant filtering can be seen in Figure 4.5. The result was a decreased noise energy as seen in the Fourier Transform of the signal as seen in

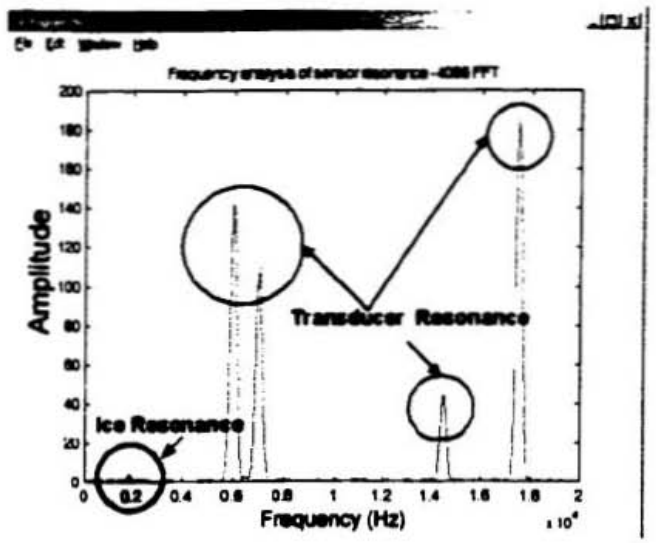

Figure 4.4: 4098 Point FFT of Simulated Signal

Figure 4.6. Notice the signal's group delay was shifted by 250 points as expected as seen in Chapter 2.

4.2.3 Time of Reflection

Unlike seismic reflections which take seconds, the time scale of reflection in ice is significantly smaller. A simple experiment was run to demonstrate the position of the first signal and the first reflection with a transducer and hammer separation of 0.7 m as seen in Figure 4.7. This geometrically calculated time delay (not including fresnel smearing) is only 50 samples apart (from Equation 4.1. In the following section, Cross-correlation will be experimented with to extract timing information.

4.2.4 Cross-Correlation

Cross correlation [20] is effective for comparing two waveforms for similarity. There is a risk that with significant decay in the reflected signal of interest and with intense resonance amplitudes, the reflected signal may not be resolvable. As seen in

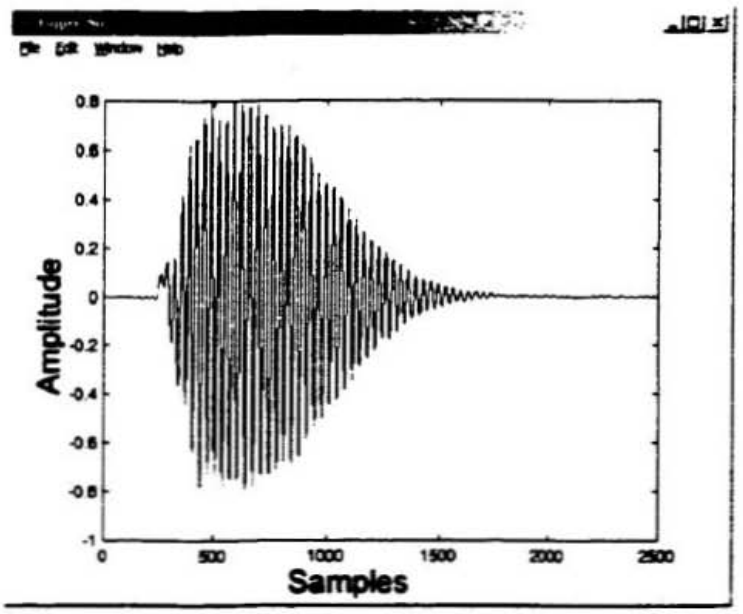

Figure 4.5: Filtered Simulated signal (190-7000 Hz)

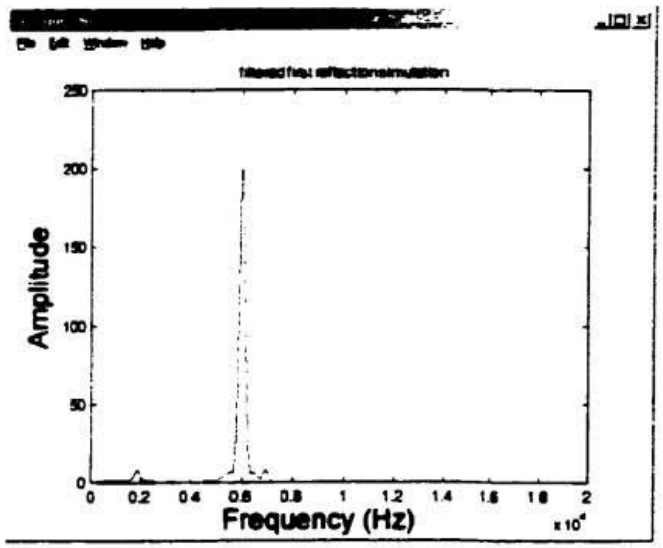

Figure 4.6: FFT of Filtered Simulated Signal (190-7000 Hz)

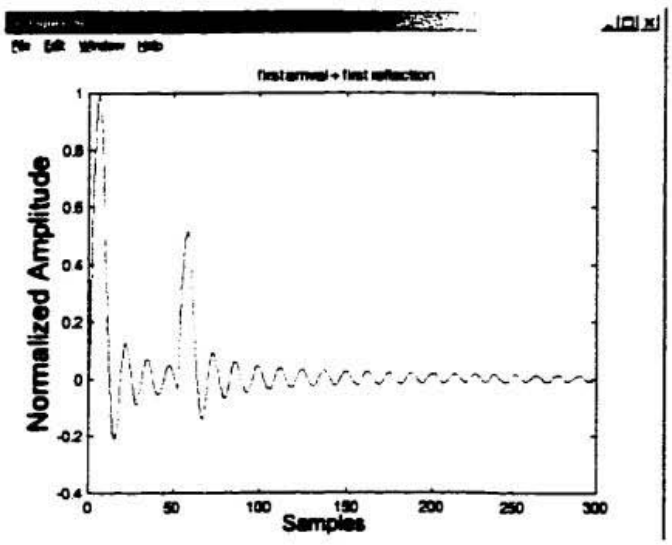

Figure 4.7: Simulated P-wave Reflection and Surface Arrival

Chapter 2. cross correlation is determined from the Equation 2.29. Once the cross correlation function was completed. a simple search for first and second maximum of the correlation was conducted. The maximums correlate to the first surface arrival and first reflection.

Figure 4.8 shows the cross correlation of the simulated signal with its self is a perfect match at 0 as expected. The first reflection placed in the data is not revealed. However. it is reasonable to expect that with more random data from the true experiments. first reflections will be more obvious. However, frequency domain will remain the most accurate measurement because of the time domain's accuracy limitation caused by the first Fresnel Zone at a frequency of 6.5 KHz.

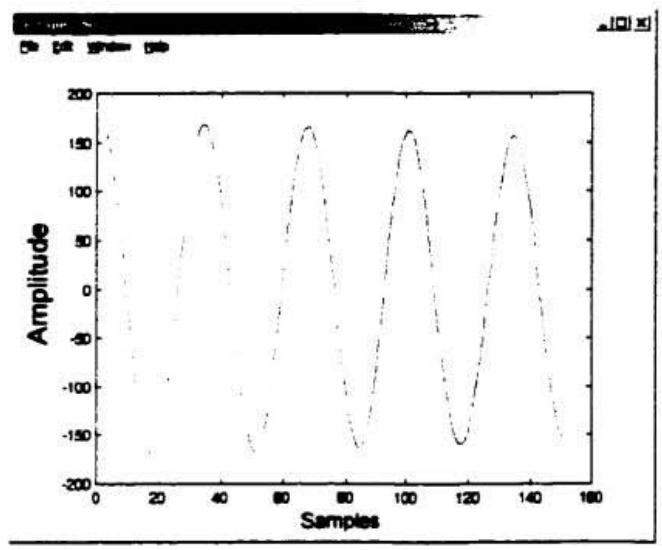

Figure 4.8: Cross Correlation of Simulated Data

4.3 Discussion and Conclusion

This simulator has proven to be an excellent tool and guide for developing an effective method of refining data processing techniques. Table 4.3 contains a list of the processes used which delivered promising indication of successful signal analysis.

From the results, there were some important observations made. First of which was a required low point Fourier Transform of 4096 points opposed to 65,000 points. As the simulated data demonstrated that the decay of the signal would only be in the order of 3000 samples, the random noise power in the remaining 62,000 samples would sum to overpower the signal of interest. The second observation is the importance of signal filtering for Cross-correlation analysis. The filtering removes corrupting data and will improve the accuracy. The third observation is the closeness of the first and second reflections, for at a depth of 1 m, the time between the reflected wave and transverse wave is only 50 samples. Cross-correlation may still be able to resolve this data though perfectly predicable data proved difficult to display the inserted signals. Higher sampling rates will decrease the error between the samples. However, the first P-wave arrival time is the most important feature for this experiment while other timing information is an asset and will only reinforce frequency domain data analysis. The total computational time of all calculations run at once on a pentium class computer was less than five seconds.

Though simulation is only an approximation of the actual signal experimentally observed, this method has proven to be an effective tool for a "heads-up" on the hurdles to overcome in the analysis of true data.

Data	First Stage	Second Stage	Third Stage	Result
Digitized Signal and Low pass analog filter (8KHz)	Multi Pole Band Pass FIR Filter	Cross Correlation	1st and 2and Max Peak	p-wave velocity and ice depth
	FFT Hamming Window	Dominant Frequency	—	Ice Depth

Table 4.3: Working Methods of Digital Signal Analysis

Chapter 5

Experimental Results

With the theory, design, and simulation preparation completed, the necessary groundwork for proving the theory as a realistic model is in place. The original goal was to determine ice properties particularly depth from acoustical impulses. But the question of where to find such ideal ice depths has not been solved. From Figure 5.1 we can see there is a "sweet spot" labelled which is the optimal location for the experiment to function.

Ice depths which are less than 0.50 m place the associated frequency range very close to the resonance frequency of the sensor, while ice depths greater than 2.0 m approach possible signal processing frequency resolving limits. This means that if a signal is sampled at 200 Khz and a 4096 point FFT is conducted, the resolvable frequency is 0.050 KHz which corresponds to a depth error of ± 0.12 m at 2 m. For proof of this concept, the specified range from Figure 5.1 represents an optimum range to begin with.

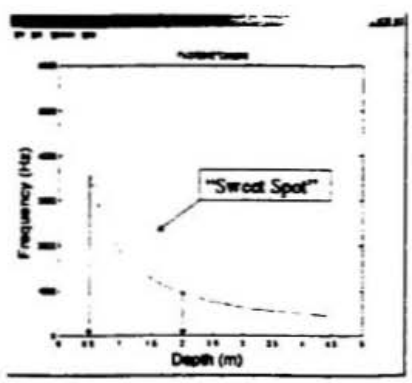

Figure 5.1: The Ideal Ice Conditions

During experimentation, two experimental expeditions were completed. The first involved artificially created granular laboratory ice at the Institute for Marine Dynamics (IMD). The second, was conducted outdoors on freshwater granular lake ice.

While this thesis does not contain experiments on sea ice, there is no foreseeable reason as to why this experiment cannot be conducted there as well.

The laboratory experiments were conducted in order to:

1. Capture timing and frequency information for a ice block.
2. Fine-tune the algorithm before going on actual field tests.
3. Debug the hardware, and evaluate system performance in cold environments.

Once the laboratory results were successfully evaluated, the ice field tests were planned. A listing of experimental data tests can be found in Appendix A as well as reasons for field experimentation location choice.

5.1 Laboratory (IMD) Experiments

5.1.1 Experiment Description and Evaluation

As specified, a block of ice thicker than 0.50 m was desired, however, in the laboratory, blocks of granular ice could only be grown to a size of 0.42 m deep X 0.32 m wide X 1.40 m long. The transducers were placed onto the center of the ice at distances 0.60 m apart using a layer of water to couple them to the ice. The blocks of ice were then lifted by crane into a large freshwater tank maintained at room temperature. Hammer strikes were made at distances of 0.65, 0.45, and 0.15 m from the first transducer. Each test was repeated a minimum of 5 times. Experiments were setup as shown in Figure 5.2.

5.1.2 Experiment Results

As this experiment was conducted on a block of ice and not an infinite plane as seen in Figure 5.3, there are 7 modes of resonance expected with a second harmonics and a possibility of the test tank itself producing resonance. Additionally, the transducer orientations can be seen in Figure 5.3. The peaks are found on the three major axis x, y , z and the minor axis on the xy, xz, yz, and xyz planes; where z is the vertical depth . Additionally, the tank where the ice block was tested had dimensions of approximately 1.5 meters deep, 3 meters wide, and 6 meters long. The tank had a

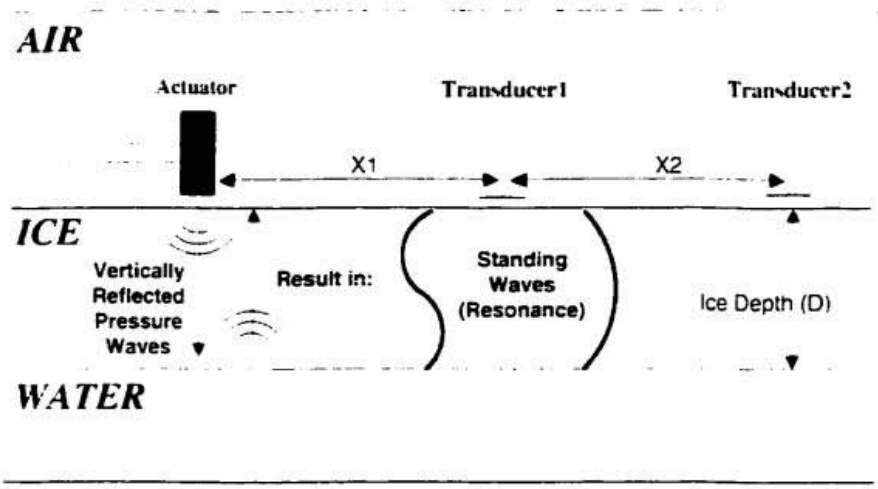

Figure 5.2: Experimental Design

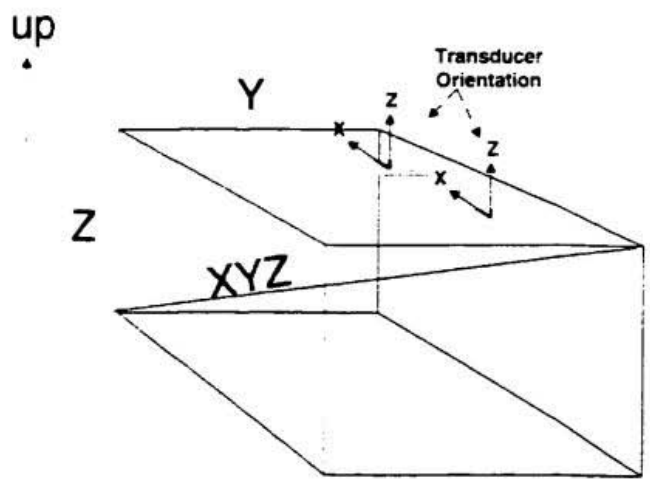

Figure 5.3: The Ice Block Dimensions and Transducer Orientation

water sound velocity of 1480 m/s. therefore tank resonance was able to be calculated using Equation 2.16. Frequencies expected with a theoretical ice acoustic velocity of 3780m/s are as follows in Table 5.1.

Substance	Mode	Dimension	1^{st} Harmonic	2^{nd} Harmonic
Ice	x	1.40 m	1.35 KHz	2.7 KHz
	y	0.42 m	4.5 KHz	9.0KHz
	z	0.32 m	5.9KHz	11.8 KHz
	xy	1.46 m	1.3KHz	2.6 KHz
	xz	0.52 m	3.57KHz	7.1 KHz
	yz	1.43 m	1.3KHz	2.6 KHz
	xyz	1.52 m	1.2 KHz	2.5 KHz
Tank	x	7.31 m	0.101 KHz	0.202 KHz
	y	1.82 m	0.411 KHz	0.822 KHz
	z	0.8 m	0.925 KHz	1.850 KHz
	xy	7.53 m	0.098 KHz	0.196 KHz
	xz	1.97 m	0.375 KHz	0.751 KHz
	yz	7.35 m	0.100 KHz	0.201 KHz
	xyz	7.57 m	0.097 KHz	0.195 KHz

Table 5.1: Expected Frequency Spectrum

In Figure 5.4 the frequency characteristics closely parallel the expected results (Table 5.1) with a dominant peak at 6.0 KHz which is near the transducer's resonance. also there is a peak at 4.5 KHz which represents the y resonance mode. Other peaks visible were the largest at 0.925 KHz for the z mode of the tank resonance and0.411 KHz for the y mode of tank resonance. Additionally. a peak at 2.7 KHz represents the x. xy. xz. and xyz second harmonics of resonance. Frequency components in the 1 KHz range overlap each other and are difficult to individually resolve. For example resonance modes x. xy. and xyz from Table 5.1 have frequencies so close together that individual peaks can not be seen in Figure 5.4.

Conversely. the timing information was difficult to determine due to the many reflections in the ice. However. with the current values. velocity can be seen with reference to the cross-correlation of the x components of transducer one and two. The time of first arrival in the x direction is slurred with the time of first reflection of the y and z direction (Figure 5.5). The vertical bar on the graph crosses the first hump of the direct path at $(1.6 \cdot 10^{-4})$ seconds. corresponding to a velocity of 3750

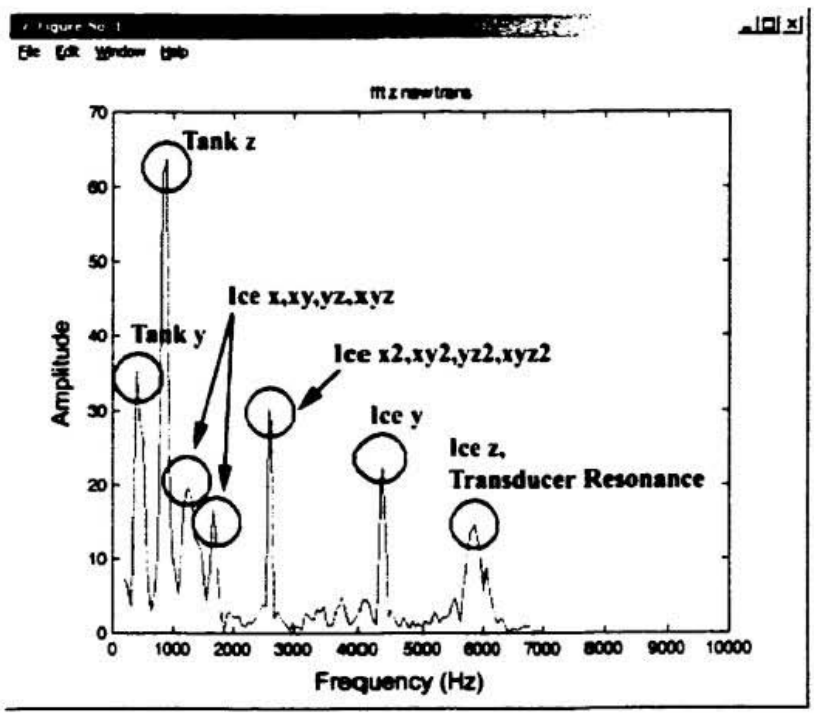

Figure 5.4: FFT of IMD Experiment

m/s. which is in the expected range.

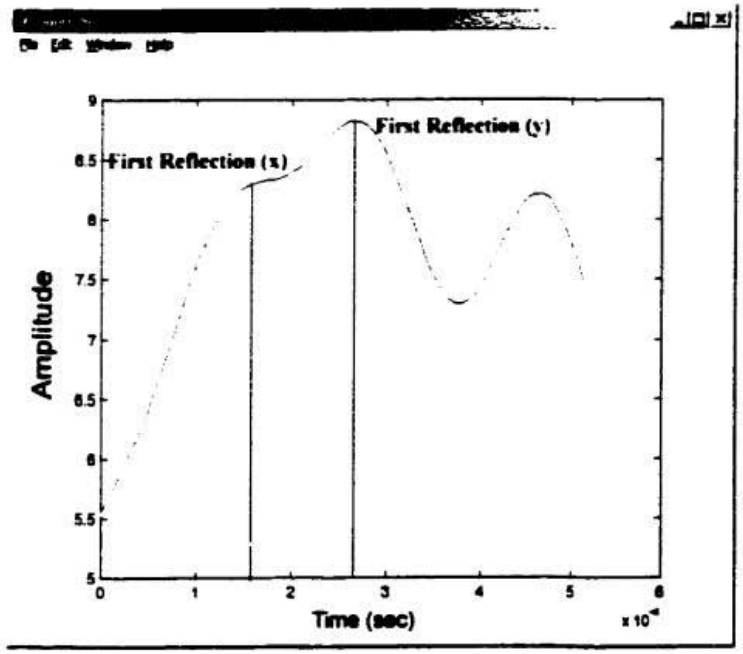

Figure 5.5: Cross-Correlation of x1 and x2 Transducers

5.1.3 Discussion

The experiment provided important information on the properties of transducer response. The first is the inter-channel cross-talk between x and z accelerometers. The signal of the first arriving surface x component wave was observed to be coupled to the vertical z accelerometer. This correlation was not revealed during calibration so one is led to believe that the reasoning for such a phenomena is the squeezing of the ice pressure wave on the transducer which results in a 3 dimensional elastic deformation of the block. In a 3D solid, the requirement that the displacements are continuous and single valued puts a constraint on the strains, known as the strain compatibility equation, and expressed in formal tensor notation as:

$$\varepsilon_{ij,lm} + \varepsilon_{lm,ij} - \varepsilon_{im,jl} - \varepsilon_{jl,im} = 0 \tag{5.1}$$

The subscripts before the comma designate the component of strain, and the subscripts after the comma show partial derivatives with respect to the indicated coordinate direction. The physical manifestation of Equation 5.1 is that a deformation in one direction is always accompanied by deformations in other directions. [24]

A similar lower timescale analogy would be a cube of $Jell - O^{®}$ being squeezed and released. The cube would deform in all 3 dimensions instead of the one dimension squeezed. When conducting field work, x and z components will now be considered similarly and not independently.

Multi-modes of reflections appeared in the system with some of the 7 predicted resonances visible. However, peaks were very close together and they were not resolvable, especially in the 1 KHz range where the lowest first three peaks represent the energy spectrums of many modes. This phenomena occurred because the frequency separation was very close to the FFT resolving limit. On field ice, this phenomenon is not expected to happen as there will be only one wave channel (other than the possibility of cracks) in which resonance can occur. Finally, the cross correlation's two interfering cycles from the y components reflection and the first x reflection interfere with each other producing visibly detectable values. Yet, as in actual field data this is expected to be more clearly defined, therefore the y component will not exist. Y component reflections were at first not expected to be resolved, however, as the transducer's coordinates were coupled, the y component is the logical expectation.

5.2 Field Tests (Moosehead Lake)

Moosehead Lake is located near Wabush, Labrador in province of Newfoundland and Labrador, as seen in the figure below. This lake was chosen due to its closeness to Wabush, its reduced chance of city pollution (minerals and heat), and most importantly, the depth of the ice which ranged between 0.51 and 0.71 m.

Depth measurements were made by drilling the ice and using a ruler-string. The snow cover was an average of 0.17 m of granular snow at an average density of 215 kg/m^3 with a standard deviation of 34 kg/m^3. The density gradient of the snow was continuous with light flakes on the top and dense icy snow found on the ice surface. The ice density in some areas (near heavily used snowmobile tracks) was 937 kg/m^3 while lesser snowmobile tracked areas had an ice density of 881 kg/m^3. However, as the theoretical maximum ice density is 920 kg/m^3 the measurement of 937 kg/m^3 indicates inaccuracy in the free-board measurement or inaccuracy in the measurement of depth.

First, the lake was surveyed for depth profiles. The deepest ice, 0.71 m, was found at the east side of the lake, in the center the ice was a depth of 0.60 m, and at the west side there was a depth of 51 cm. Although difficult to detect, the under ice profile was suspected to vary locally. Therefore the ice was profiled 5 times in a circumference of 5 meters (center, and 4 perpendicular corners), the variation in depth was up to ± 4 cm. The measured depth of the lake at all test points was found to be greater than 6 meters. The temperature ranged from -30 to -15 °C, and at the surface of the ice (probed through the snow) the temperature was found to be -8 °C.

5.2.1 Experiment Description

Experiments were conducted over a series of 4 days in a consistent manner. Two transducers were frozen with cool water from a thermos to the ice with a separation of 0.60 m at a magnetic N-E orientation. The reasoning for the N-E orientation was that N-E is parallel to the shape of most cracks on the lake that were every $2 \rightarrow 5m$. The hammer strike was made at a distance of 0.60 m in 4 points around the sensors (Figure 5.6). Other experiments conducted included different orientation of the sensors and hammer strike locations of up to 3.5 m. The varying strike locations were performed in order to investigate how impact location affected frequency response, as well as to verify the cross-talk of the transducers. Each strike was repeated 5 times at each location.

Figure 5.6: Experiment Setup,(X=Strike Pts)

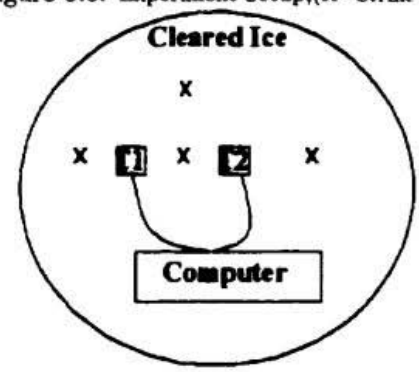

5.2.2 Time Evaluation

Each experiment was processed with a 500 pole band pass FIR filter between 0.5 Hz and 6.5 KHz, followed by a cross-correlation. A search for the cross-correlation maximum and second maximum sample count was made between transducer 1 and transducer 2. From the first maximum, the velocity was calculated. Then with a cross-correlation of transducer 1 with itself, depth can be determined. Figure 5.7 is an example of cross-correlations of the first transducer with the second transducer over a series of tests which were then overlapped upon each other and graphed for visual comparison. The dominant signal corresponds to the first P-wave time difference from the first transducer. The crossing happened at an average of 42 samples after the initial. The velocity was calculated to be 3600 m/s for 0.51 m, 3810 m/s for 0.60 m, and 3650 for 0.71 m with an error of ± 100 m/s . The 0.6 m site was heavily travelled upon by snowmobiles and was oriented in the lake center where as 0.71 and 0.51 m were both at the lake edges and had little snowmobile travel.

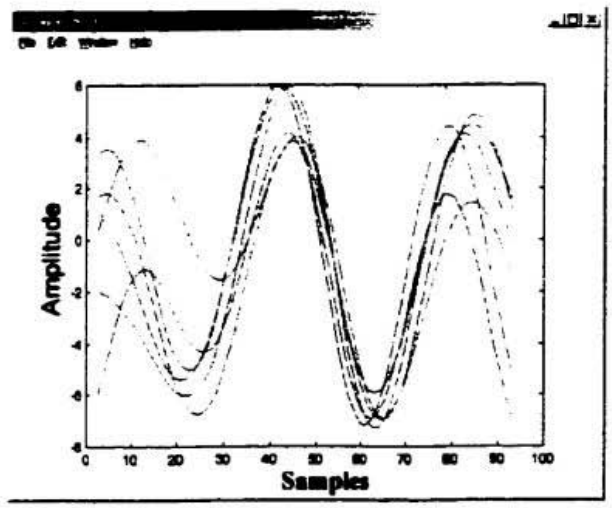

Figure 5.7: Velocity Cross Correlation of Transducer 1 with 2

Once the velocity was calculated, transducer 1 was cross-correlated $\propto x$ to determine an ice depth-time correlation. This experiment was automated to collect data from groups of the six cross-correlating experiments adding all six cross-correlations together, and then a search for the second maximum peak was conducted. The results of the 0.60 m cross-correlation are described in Figure 5.8 with the experiment setup.

The time difference was calculated from the geometric difference of the first arrival time from the first reflection time as follows in equation 5.2 where HT_{sep} is Hammer-Transducer separation.

$$\Delta Samples = \frac{(\sqrt{d_{ice}^2 + (\frac{1}{2}HT_{sep})^2} - HT_{sep}) \cdot SamplingFrequency}{V_{ice}} \tag{5.2}$$

The results are summarized in Table 5.2. Note that in Table 5.2 title **Actual Value** refers to characteristics directly determined. For example, P-wave velocity was used as a typical velocity in fresh water ice and the depths were determined by drilling through the ice sheet. Additionally, the title **Experimental Values** refers

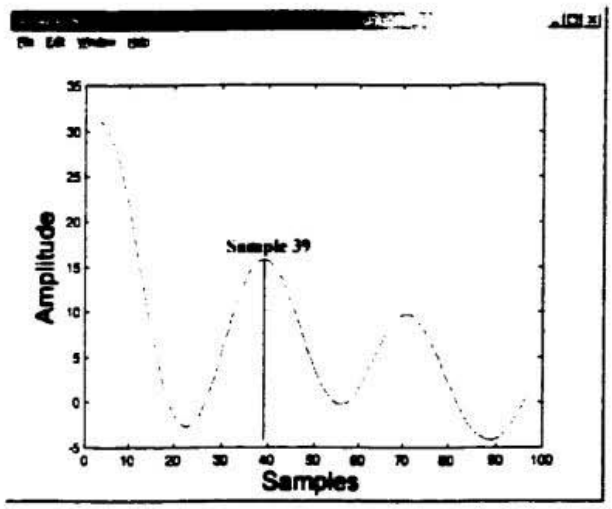

Figure 5.8: Cross-Correlation Summing of 5 Tests at 60 cm

to cross-correlated data measured with the sensors.

Measurement	Actual Value	Experimental Values	% Error
P-wave Velocity	3780 m/s	3750 m/s	0.8 %
Cross-Correlation	71 cm	67.8	4.4 %
	60 cm	58.5	2.5 %
	51 cm	64.6	21 %

Table 5.2: Cross Correlation of Experimental Data vs True Values

5.2.3 Frequency Evaluation

To reduce the random noise and augment non-random signals with each depth measurement (each hammer strike), groups of 10 data set's x and z frequency components were summed together [16]. However, as seen in Figure 5.9 (0.71 m) the decay of the impulse signal occupies less than 1000 samples, a danger existed that the 4096 points of data would collect too much noise power and corrupt the results. Therefore the experiment was reduced to a 2048 point FFT (compared in Figure 5.10) which has a stronger peak.

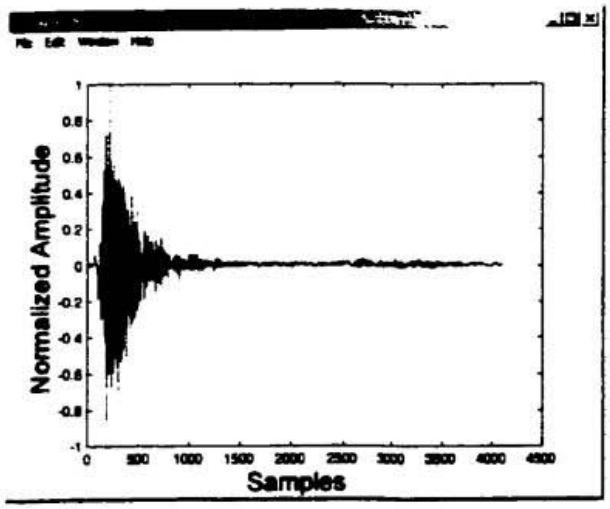

Figure 5.9: Typical Moose Lake Signal Decay

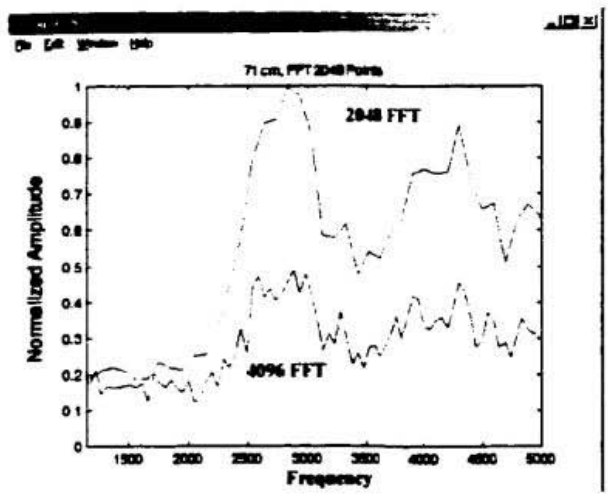

Figure 5.10: 2048, 4096 Point FFT Comparison

The data for all three different depths was then evaluated using this methodology (Figure 5.11). The first dominant frequency peaks will correspond to each of the depths. Higher frequency peaks are results from impurities in the ice such as cracks. The dominant frequency peaks for depths of 0.71, 0.60 and 0.51 m are 2800, 3000, and 3200, respectively. To view a collection of some individual results of each experiment, go to Appendix B. As determined in the previous section, the velocity of a P-wave in ice is 3750 m/s. Substituting the dominant frequencies and velocity into Equation 1.6, the corresponding results as compared to the physical measurements can be seen in Table 5.3.

Measurement	Actual Value	Experimental Values	% Error
Depth (frequency domain)	71 cm	67 cm	5.6 %
	60 cm	62 cm	3.2 %
	51 cm	58 cm	12 %

Table 5.3: Frequency Correlation to Actual Values

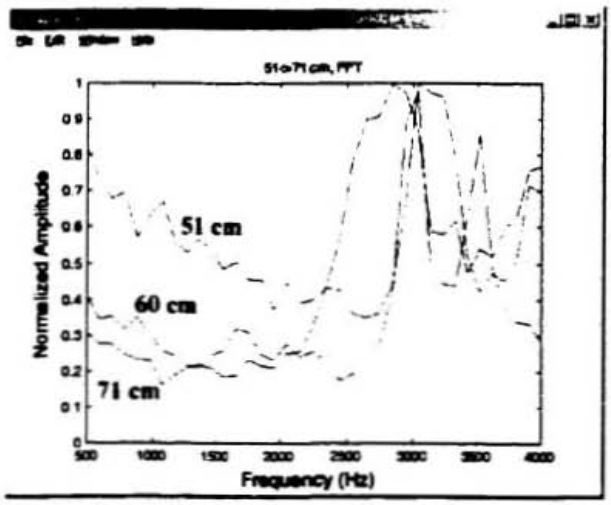

Figure 5.11: Frequency Evaluation of 3 Depths 71, 60, 51 cm

5.3 Error Analysis and Anomaly Discussion

An analysis of the accumulative error system will further verify the validity of the tests and build a basis for future designs to consider. The sources of error in this experiment can be generalized into three specific areas: physical properties of ice mechanics, sensor characteristics, and signal processing. The following sections evaluate such characteristics of the experiment.

5.3.1 Physical Characteristics

Before starting the physical characteristics, a brief list of some terms will be defined in the following list.

Frazil: super cooled water, often moving, forms into tiny, randomly oriented, spherical crystals under ice sheets.

Large Cracks: cracks with visible air spaces.

Small Cracks: small meaning visible with no air space.

Floating ice is subject to many environmental disturbances. Water currents are almost always present in the ocean and also very common in lakes. Currents cause "frazil" build-up and non-uniform subsurface ice formation. As well, currents and thermal expansion produce forces on the ice's horizontal axis which results in a constant appearance of cracks. Since snow has a typical density of 250 kg/m^3 its weight adds a substantial vertical pressure to the ice and also causes cracks. Figure 5.13 is an example of below ice surface variability in the Arctic Ocean.

In the case of the experiments conducted within this thesis, the laboratory experiments were conducted on crack-free ice. Whereas ice in the field experiments was composed of of bubbles and vertical cracks which frequently appeared. Attempts were made to avoid large cracks, however crack avoidance proved difficult and experiments were conducted near large cracks (within 1 meter) and over some small cracks. Core samples were a considered possibility for ice characterization, however a bubble distribution would not effect the experiments as the lowest frequency will always be the bottom of the ice and second order ice dynamics are negligible.

However. the most noticeable variability effects on ice measurements was thickness variability of the subsurface planes and "icy" snow on the ice surface. As explained in "The Moosehead Lake" experimental procedure. the ice depth in the 60 cm area varied by and absolute error of $\pm 4cm$. As the experimental value of the V_{ice} is $3810 \pm 100m/s$ the error can be calculated from the frequency-depth formula 1.6 (Equation 5.3). resulting in the values seen in Table 5.4. Extra notice should be paid to the error of measurement which increases as the depth of the ice decreases.

$$\delta f = \sqrt{(\frac{\partial f}{\partial d_{ice}}\delta d_{ice})^2 + (\frac{\partial f}{\partial V_{ice}}\delta V_{ice})^2} \tag{5.3}$$

Depth	Error
71 cm	$\pm$ 0.160 KHz
60 cm	$\pm$ 0.220 KHz
51 cm	$\pm$ 0.302 KHz

Table 5.4: Frequency Error

The tests suggest that the ice in Moosehead Lake is nonuniform below the footprint covered. The footprint of resonance below the test area can be determined. from the Fresnel zones of the ice depth.

Large *air* filled cracks would pose a definite signal boundary. however. smaller cracks are also not a perfectly cleaved surface and the horizontal plane would also be under compression. Yet a signal can still travel through them. In reference to the experimentation. there is no detectable evidence that the cracks had any affect on the results.

However the effects of bubbles and small bubble density are wavelength dependant. Acoustic wave scattering can occur from bubbles. however. the advantage of resonance measurement is that the lowest resonance frequency will indicate the depth of the ice and the bubble clouds will be seen as higher frequency harmonics (Figure 5.12).

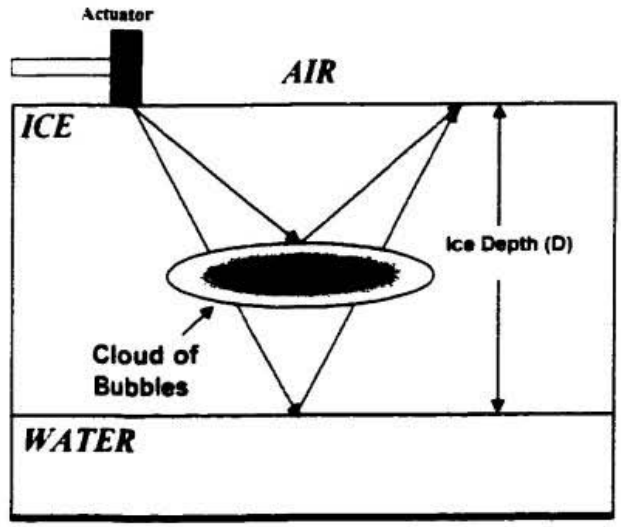

Figure 5.12: Bubble Clouds In Ice

5.3.2 Signal Processing Limitations

Fourier Transforms have a limited resolvable frequency. To capture a frequency resolution of less than 0.050 KHz/point the Fourier Transform will have to extend into the *no-signal* region where the noise of the instruments will begin to dominate the measurement. Therefore, the error in measurement grows at lower frequencies (Equation 5.4). The FFT error on experimental depth are explained in Table 5.5.

$$\delta d = \sqrt{(\frac{\partial f}{\partial f}\delta f_{FFT})^2 + (\frac{\partial f}{\partial V_{ice}}\delta V_{ice})^2} \tag{5.4}$$

Timing errors are caused by a sampling discretisation error, which is a simple calculation of error/sample. For instance, the error in the velocity Equation 5.5 calculation can be seen in Equation 5.6. With the experimental sampling frequency of 200.000 KHz/sec, the difference corresponding to one sample causes an error of ± 72 m/s that is determined through Equation 5.6 and corresponds closely to the statistical experimental error of $\pm$ 100 m/s. The value of this error indicates that

Depth	Error	% Error
0.71 m	± 0.02 m/point	2.8 %
0.60 m	± 0.015 m/point	2.5 %
0.51 m	± 0.011 m/point	2.1 %

Table 5.5: FFT Error

the limitation of this measurement is caused by slow sampling frequency.

$$V = \frac{d}{t} \tag{5.5}$$

$$\delta V = ABS(\frac{\partial V}{\partial t}\delta(1/f_{sampling})) \tag{5.6}$$

The error in a one sample delay for depth readings can be calculated from Equation 5.7 as seen in Equation 5.8. With a time between each sample at of 1/(sampling frequency) and depths of 0.51, 0.60, 0.71 m, the resultant errors are shown in Table 5.6.

$$D_{ccr} = \sqrt{(\frac{\Delta t V_p}{2})^2 - (\frac{X_1}{2})^2} \tag{5.7}$$

$$\delta D_{ccr} = \frac{\partial D_{ccr}}{\partial \Delta t}\delta \Delta t \tag{5.8}$$

Depth	Error	% Error
0.71 m	±0.087 m/point	1.19 %
0.60 m	±0.082 m/point	1.35 %
0.51 m	±0.077 m/point	1.4 %

Table 5.6: Timing Reflection Error

The final error to discuss is the the Fresnel Zone error. The fresnel zone [16] states that the resolving time capability can be no greater than r_f as described in Equation 2.13. As the signal for Cross-correlation is filtered at 6.5 KHz, the vertical resolvable limit, r_f, in the time domain is 0.14 m.

5.4 Conclusion

Frequency and time evaluations demonstrated consistent results between the cross-correlation and Fourier Transform. which included an incorrect high frequency and time correlation at a depth of 0.51 m. This measurement of 0.51 m was made within 100 m of the shore and in line with a brook which could be an indication that ice frazil or other deposits may have collected at the bottom of the ice. Additionally. frequency peaks are not sharp which indicates a possible variation in the ice bottom layer shape. This is very common for sea ice and is possible for lake ice if there is significant moving current below the ice. Frazil buildup was suspected as the profiling measurements around each site revealed a $\pm 0.025m$ variation and a feeder stream was nearby. Figure 5.13 is an extreme example of such variations in ice layers and frazil buildup on the ocean bottom of arctic sea ice.

Figure 5.13: Under Ice - Arctic Ocean

This method of resonance has proven a viable technique for the determination of ice depth and ice block characteristics. Timing calculations required high sampling frequencies in order to calculate correct errors. However, frequency analysis was able to sample effectively at much lower frequencies. Cross-correlation in the time

domain is an extremely useful function as its results are not dependant on signal amplitude but signal shape. However, because x and z components on each sensor were discovered to be coupled when frozen onto the ice surface, one component was disregarded meaning that higher sampling frequencies could be used. With the reduction of each transducer's z component, the opportunity exists to either extend the sampling frequency to 400 KHz, or to add two more transducers to increase the data's accuracy.

One remaining point of interest is the difference between the resonance bandwidth in the "perfect" ice block created in the laboratory and the field ice blocks. The frequency content of "perfect" ice had a sharp bandwidth of less than 0.20 KHz while the FFT limitation was 0.050 KHz/point implying a sharper peak than visible (Figure 5.4). Conversely, the resonance peaks found in the field exceeded 0.50 KHz, suggesting a nonuniform bottom in the footprint area.

These results suggest the authenticity of the resonance calculation, and further experiments to complete a full evaluation of different depths would be an asset for this topic.

Additionally, error analysis has indicated that the sources of error are in the actual variations of the ice depths $\pm 0.04m$ which resulted in a broad frequency peak for each depth instead of a distinct sharp point. As well, the Fourier Transforms have an error region of up to 0.025 m and a timing error of up to 0.0087 m. However, with the error of velocity included in this measurement, the result is increased to a value of 0.02 m. Yet, the primary limitation remaining is still the Fresnel Zone limit of 0.042 m. In summary, the errors of this experiment are most significant within the Fresnel limitation, Fourier Transform limitation (caused by sensor noise), and within the sampling frequency.

Chapter 6

Conclusion

In previous reports, [1] [2] acoustic analysis of ice depth was determined to be feasible, although at the time of such reports, analysis had never been attempted. In this thesis, the evaluation of ice depth through acoustic analysis has proven to be a viable method. As well, the refinement of instrument and computer technology has reached a level where acoustic sensing instruments deliver precise data in regards to ice vibration measurements.

Fulfilling each of the target objectives incorporated a successful execution of theory, development, simulation, and experimentation; where each stage was dependant upon the completion of the previous stage. In review of the target goals of this thesis, the target goals accomplished were to:

1. Mathematically prove ice resonance and time reflections are a viable method to determine ice properties.
2. Develop a method of instrumenting ice vibrations.
3. Create software for the data acquisition system.
4. Collect experimental data on actual ice.
5. Develop a functioning algorithm to automatically calculate ice properties.

The ice resonance method proved successful as an excellent method in determining ice depths. Where Equation 2.16 and Figure 2.3 indicate that the acoustical range between 0.2 and 10 KHz corresponds to an ice depth of 0.2 m and 10 m of ice.

Once this was established theoretically, it was further proven experimentally, using a frequency bandwidth of 8 KHz, and a sampling frequency set at 200 KHz.

Reflection energy loss was calculated using Equation 2.9 where this was a good estimation due to the sensors being capable of resolving the ice resonance power. The reflection and the transmission coefficients were calculated and can be seen in Table 2.3. The values in Table 2.3 indicate that poor air coupling of a transducer, as well as an actuator to the ice surface must be eliminated for this experiment to be viable. The freezing of the transducers to the ice surface accomplished this.

The experimental setup was capable of achieving a large portion of the requirements. The critical successes are the sensor bandwidths and multi-channel, high frequency sampling. All other requirements either exceeded or were quite close to the required specifications. Two such components of the design which were inferior include the impact senor saturation and the signal to noise ratio of the transducers. Furthermore, preliminary experiments met the needed specifications, the ability of the system to resolve ice resonance was able to be proven on actual ice sheets.

Additionally, LabView, the choice of data acquisition software was ideal for this application. LabView's hardware accompaniment was capable of both undergoing quick experiment setup and last minute alterations.

A particularly interesting point to note is the receival method of the data files to the post processing program: Matlab. The data file's header information starts each line with % until the first line of actual data begins where the text: '**A**=[' is placed that signifies the start of the Matlab matrix. Also, the last two characters in the matrix are '];' which signify the end of the matrix. The advantage of this file type is that a data file is able to be imported directly onto Matlab as a matrix 'A' simply by typing "data_file_name.m" at the Matlab prompt.

The simulator has confirmed to be an excellent tool and guide for the development and an effective refinement method of data processing techniques. Table 4.3 contains a list of the processes used which delivered promising indication of successful signal analysis. From the results, there were various important observations that were made the first of which was that a required low point Fourier Transform of 4096 points opposed to 65,000 points was needed, coinciding to what was previously expected. Also, the simulated data demonstrated that the decay of the signal would be in the order of 3000 samples, yet the residual the random noise power in

the remaining 62.000 samples summed to a number over the power spectrum of the signal of interest. The second observation stresses the importance of signal filtering when dealing with correlation analysis. The filtering removes all corrupting data and. therefore. improves the accuracy of the correlation by eliminating non-signal oscillations. The third observation is the closeness of the first and second reflections. for at a depth of 1 m. the time between the reflected wave and transverse wave is only 50 samples. Cross-correlation was capable of resolving this data. however. during simulation of this data. cross-correlation proved to be not effective with the inserted artificial signals. Although simulation is only an approximation of the actual signal experimentally observed. this method is an an effective tool for an insight in the analysis of true data.

Frequency and time evaluations also demonstrated consistent results regarding the cross-correlation and the Fourier Transform such as an incorrect high frequency and time correlation at a depth of 0.51 m. This measurement of 0.51 m was made within 100 m of the shore and in line with a brook. which is believed to be an indication that ice frazil or other deposits had collected at the bottom of the ice. Moreover. frequency peaks were not sharp. indicating a possible variation in the bottom layer shape of the ice. For most ice. this is common and is in correspondence to measurements which show a $\pm$ 0.025 m variation. Figure 5.13 is an example of such variations in ice layers with frazil buildup on the ocean bottom of arctic sea ice.

This experimentation using ice resonance has proven to be a good technique in the determination of both ice depth and ice block characteristics. Timing calculations required high sampling frequencies in order to calculate the correct errors. However. frequency analysis was able to be sampled effectively at lower frequencies. Cross-correlation in the time domain was an extremely useful function whereas its results are not dependant on signal amplitude. but on signal shape. Yet. because x and z components on each sensor were coupled together when frozen onto the ice. one component was disregarded which means that a higher sampling frequency was able to be used. With the reduction of each transducer's z component. the opportunity existed to (a) extend the sampling frequency to 400 KHz. or (b) to add two more transducers which would increase the data's accuracy.

A final point of interest involves the difference between the resonance bandwidth in the "perfect" ice block (created in the laboratory) and the field ice. The frequency

content of "perfect" ice had a sharp bandwidth being less than 0.20 KHz. while the FFT limitation was 0.050 KHz/point this implied a sharper peak than was visible (Figure 5.4). Conversely, the resonance peaks found in the field exceeded 0.50 KHz. suggesting a nonuniform bottom in the footprint area. Error analysis indicated that the sources of error were in the variations of the ice depths ($\pm 0.04m$). Moreover, the significant errors encountered were the Fourier Transforms that had an error region of up to 0.025 m and a timing error of up to 0.0087 m. Yet, the primary timing limitation remaining was still the Fresnel Zone limit of 0.14 m. In summary, the errors found in this experiment are most significant within the Fresnel limitation. Fourier Transform limitation (caused by sensor noise), and within the sampling frequency.

Timing and resonant methods were proven theoretically and practically. Additionally, effective instruments were developed for accurate analysis of the required specifications. The opportunity exists for further development of a device which is hand-held and therefore a marketable product. A marketing assessment is beyond the scope of this thesis, the opportunity remains for future experimentalists to consider.

Chapter 7

Future Research

The data collected in this experiment proves that ice profiling through resonance and time measurements is a viable method for routine, practical and industrial use. However, improvements and other experiments can still be made to the original transducer design. Further testing using the existing setup will continue to push the experimental refinements as close as possible to a final product. Additionally with the analysis of depth, analysis of each individual transducer could be made instead of stacking all components of all transducers together.

Limitations encountered during the experimentation dealt primarily with the resonance of the transducers and the signal to noise ratio. To reduce these shortcomings, a higher order analog filter can be utilized to aid in the signal saturation produced by resonance. Careful experimentation should be conducted with a simple transducer so that further reduction of its signal to noise ratio can be achieved. For example, by placing the capacitor banks closer to the power and ground lines a further reduction of noise may occur.

Future designs should also consider the cost effectiveness of a "laser optical vibration measurement system" which will produce a virtually noise free and linear signal. The usage of different material types to reduce the transducer size and transducer's support frame may reduce this resonance problem. For example, this could be achieved by sealing the electronics in epoxy resin instead of a milled plastic block. To further prove this methodology an extension of the current experimental data pertaining to first-year and multi-year sea ice and a depth range beyond 1 m of ice is required.

Cracks and bubbles appear to cause little degradation of the tested signals, however, variable frequency experiments on cracked and bubbled ice may reveal the transparency of crack and bubble boundaries.

Finally, software automation development would be an asset for future researchers in this field. For example, in this experiment data was collected and preprocessed in LabView followed by further processing in Matlab. If this system were to be developed into a single software instrumentation package in C++ and then imported into LabView so that a final hardware implementation could be developed, the recovery of data would become much quicker and more efficient.

7.0.1 An Experiment With Wavelet Analysis

An extension of Cross-correlation, and the Fourier analysis theory is the Wavelet Theory. Wavelets are commonly used in seismology to extract timing and frequency information from a signal buried in noise. Therefore, wavelet analysis seems to be the most appealing choice for use in experimentation. A diagram of time vs frequency is shown in in Figure 7.1.

Research was conducted using simulated data experiment in efforts to extract timing information. The base wavelet chosen to use was the Daubechies 29 wavelet because of its linear phase delay and low pass filtering characteristics.

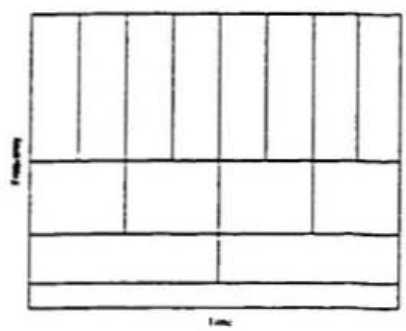

Figure 7.1: Wavelet: Frequency vs Time

The Continuous Wavelet Transform (CWT) was developed as an alternative approach in overcoming the resolution problem of the Short Time Fourier Transform (STFT). The CWT analysis is carried out similarly to the STFT analysis, in that the signal is multiplied with a function (similar to the window function in the STFT). Additionally, the transform is computed separately for differing segments of the time-domain signal. However, there are two main differences between STFT and CWT:

1. The Fourier Transforms of the windowed signals are not taken, and therefore,

a single peak will be seen as corresponding to a sinusoid (i.e. negative frequencies are not computed).

2. For CWT, the width of the window is changed as the transform is computed for every individual spectral component. This is the most significant characteristic of the Wavelet Transform.

The continuous wavelet transform is defined as follows:

$$CWT_x^{\psi}(\tau, s) = \Psi_x^{\psi}(\tau, s) = \frac{1}{\sqrt{|s|}} \int x(t) \psi^* \left(\frac{t - \tau}{s} \right) \partial t \qquad (7.1)$$

As seen in the above equation , the transformed signal is a function of two variables, τ and s , the translation and scale parameters, respectively. $\psi(t)$ is the transforming function and is called the "Mother Wavelet". The wavelet function is a built-in feature of Matlab.

Using the simulated data, the known insertion impulse is a 5 KHz sine function. Therefore an expected strong correlation to the reflected data is on wavelet number 20 and above (100.000/5.000 = 20) when using wave number in the wavelet decomposition. However, upon examination, the wavelet analysis was too noisy to be able to retain any reliable information (Figure 7.2). The reason for this being that the filtering of the Daubechies Wavelet is not a perfect low pass filter and results in corruption from the inserted resonance. There are many other types of wavelets that could be used, and a thorough investigation of different wavelets may reveal interesting results.

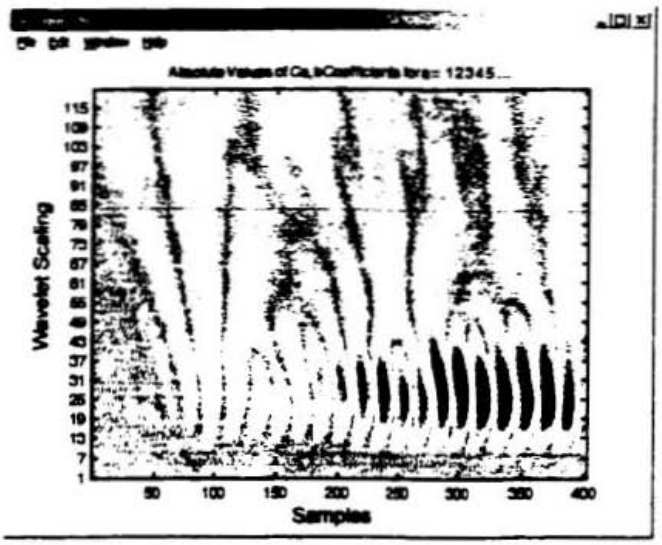

Figure 7.2: Wavelet Experiment Data

Appendix A

Field Test Description

A.1 Institute of Marine Dynamics

A.1.1 Environment

The Institute of Marine Dynamics (IMD) is located in St. John's. Newfoundland. Canada. The facilities available at the IMD consisted of a cold-room. a small ice growing tank. and a pool of room temperature freshwater. A photograph of the ice block prior to being lifted into its tank is shown in Figure A.1.

A.1.2 Experiment 1 Procedure

The ice tank was filled with freshwater and left in the cold-room at a temperature of -20 C for 10 days in order to achieve a maximum ice thickness of 0.42 m. The progress of the freeze was monitored periodically by drilling into the ice block. The type of ice created by this method was granular. The quality of the ice was virtually bubble free. without any visible cracks.

Once the ice was frozen to its maximum thickness. transducers were frozen to the top of the ice. This was achieved by pouring a small amount of water onto the ice surface followed by placement of the transducers onto the ice. When water was poured onto the ice. the ice cracked locally in approximately a 0.10 m diameter area. The transducers were placed 0.60 m apart and were not moved from their original position. Hammer strikes occurred at distances of 0.15. 0.30. and 0.60 m.

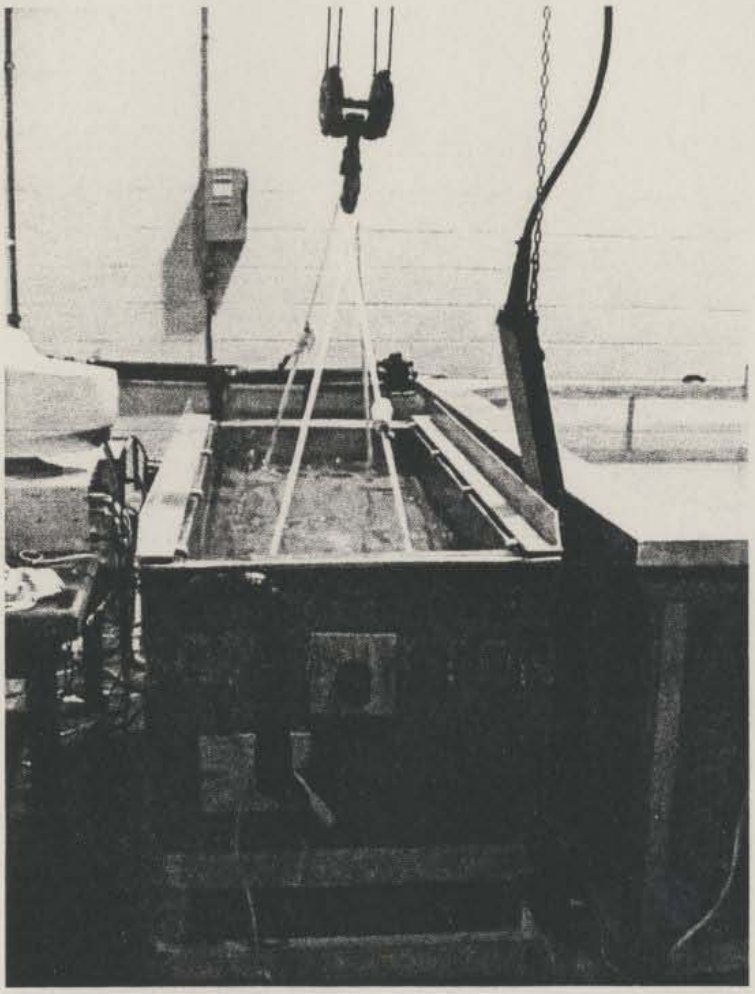

Figure A.1: Ice Block at IMD

The hammer strikes caused considerable local cracking of an area of approximately 10 cm in diameter. The frozen transducers demonstrated excellent acoustic coupling to the ice surface. In this cold environment, the transducers and the electronic cabling functioned consistently.

A.1.3 Experiment 2 Procedure

As in Experiment 1, the ice tank was again filled with freshwater and left in the cold-room under the same conditions in order to achieve a maximum ice thickness of 0.42 m. The type of ice created by this method was, as in Experiment 1, granular. Again, the quality of the ice was virtually bubble free without visible cracking. However, in this experiment, the ice tank contained side and bottom heaters that were used to ensure a linear freeze from the ice bottom.

Once the ice was frozen, the ice tank was taken out of the cold-room and maintained at room temperature for 24 hours with the tank's heaters on. The heaters served the purpose of melting the sides of the ice block so that it could be lifted out of the tank by crane (Figure A.1).

The transducers were placed on the ice 0.60 m apart. Due to the ice being at room temperature the transducers were not able to freeze to the surface and remained coupled only by a thin layer of water. The transducers remained in their original position through out the experiment.

Hammer strikes occurred at distances of 0.15, 0.30, and 0.60 m. The hammer strikes, again, caused local cracking in an approximate diameter of 0.10 cm. The transducers demonstrated excellent acoustic coupling to the ice surface, as well they appeared to resonate.

A.2 Moosehead Lake

A.2.1 Test Description

Moosehead Lake was chosen as the location of this experiment due to for its ideal ice conditions of 0.5 to 0.7 m and excellent accessability. Moosehead Lake is located at 53°70' East and 67°52' North.

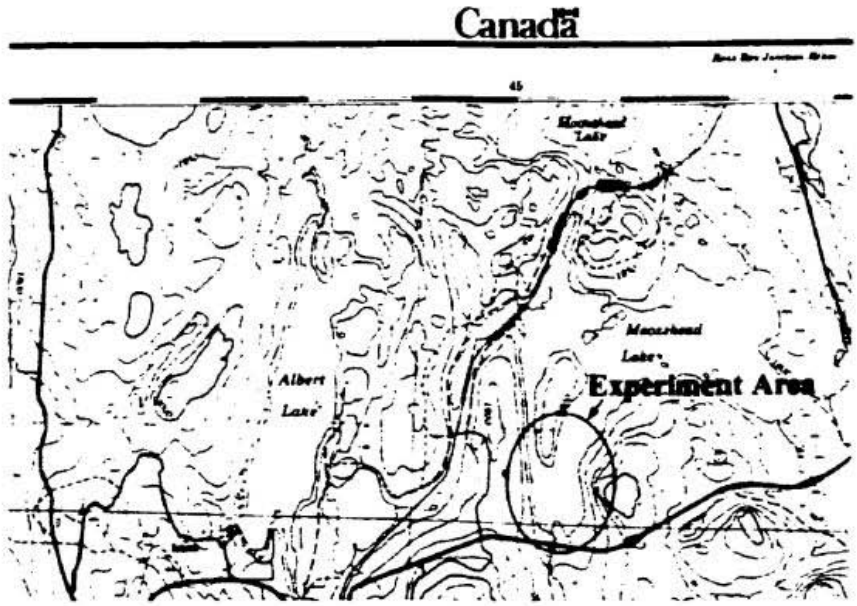

Figure A.2: Moosehead Lake

Site: X_1	Date	20-Jan-01
	Air Temperature	-23 C
	Ice Surface Temperature	-8 C
	Ice Density	$937 kg/m^3$
	Density Method	Freeboard
	Ice Depth	0.6 m
	Snow Density	$206 kg/m^3$
	Skidoo Traffic	High
Site: X_2	Date	22-Jan-01
	Air Temperature	-15 C
	Ice Surface Temperature	-8 C
	Ice Density	$858 kg/m^3$
	Density Method	Freeboard
	Ice Depth	0.71 m
	Snow Density	$238 kg/m^3$
	Skidoo Traffic	Low
Site: X_3	Date	23-Jan-01
	Air Temperature	-15 C
	Ice Surface Temperature	-8 C
	Ice Density	$881\ kg/m^3$
	Density Method	Freeboard
	Ice Depth	0.51 m
	Snow Density	$244 kg/m^3$
	Skidoo Traffic	Medium

Table A.1: Site Experiment Data

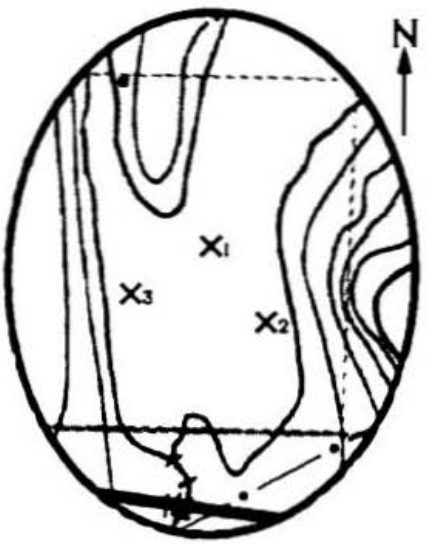

Figure A.3: Moosehead Lake Experiment Area. X Marks the Test Spots

ITEM	GEAR	BRAND	MODEL
ice thickness survey			
	big auger	spare blades	Mora 150mm
	small auger	Kovacs	50 mm
	power head		
	survey tape	Yeron	50 m
	compass		
	thickness tape		
ID0-ice density			
	electronic balance		
	calipers		
	mitre box		
	hand saw	CanTire	cross cut
	dunk bucket		
	meter stick (freeboard)		
IS0-ice structure			
	thermocouple module	Fluke	80TK
	digital multimeter	Fluke	20S
	light table and accessories	NRCC	custom
	hot plate	Thermodyne	
	glass plates		
	squeeze bottles	labwear	
	camera	Digital	
	table tripod		
	sample bags - assorted sizes		
	plastic ruler for photos		
ST0-snow thickness survey			
	metre stick		
SD0-snow density			
	snow sample pusher	custom	
	tape measure		
	graduated cylinder		
SS0-snow structure			
	hand held magnifying glass		
	grid for photos		
	close-up lense for camera		
GE0-general electrical gear			
	orange extension chord (2)	CanTire	25 m
	black extension chord	CanTire	3 m
	generator		1 KW
	power bar	Realistic	6-120V
	data storage media		
GF0-general field gear			
	field books	Wade	waterproof
	retort stand	labwear	40cm
	toolbox	CanTire	med
	ropes	CanTire	3 m, 5 m
	ice chisel		
	bungee chords and tie downs	CanTire	
	C-clamps	CanTire	
	equipment manuals		
	thermos		
	spark plugs for power head		
	gas can	CanTire	20 litre
PF0-personal field gear			
	insulated boots		
	parka and pants	Millet	
	coveralls	Workwear	
	insulated coveralls	HellyHansen	
	work gloves		
	insulated rubber gloves		
	sunglasses		

Table A.2: Mooselake General Equipment List

Appendix B

Individual Transducer Data From Moosehead Lake

General seismological theory [16] suggests adding multiple transducers and multiple tests together to reduce transducer error and random noise. However, for general interest, below is a comparison of the two transducer frequency responses on 0.71 m, 0.6 m, and 0.51 m ice depths.

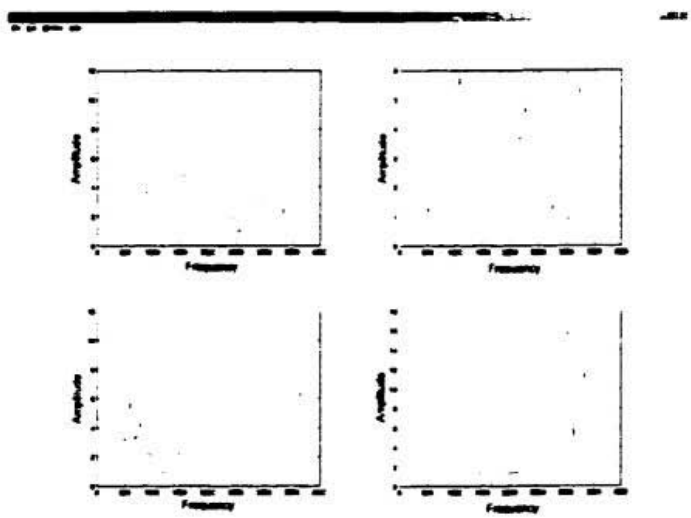

Figure B.1: Four Individual X Components of 0.51 m Resonance Data (Set 1)

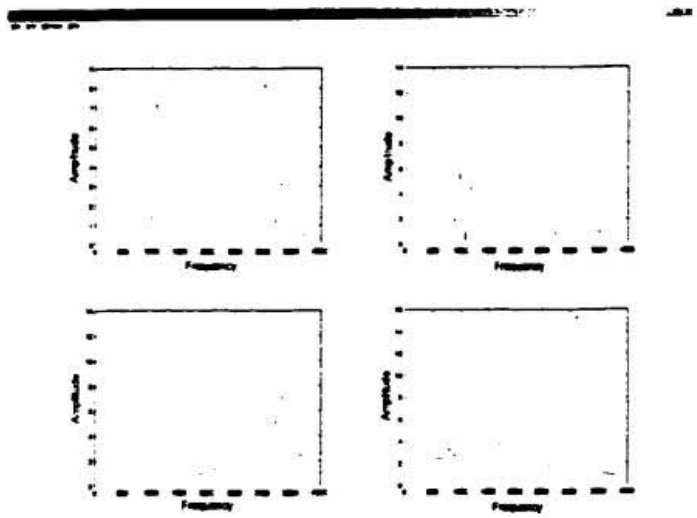

Figure B.2: Four Individual X Components of 0.51 m Resonance Data (Set 2)

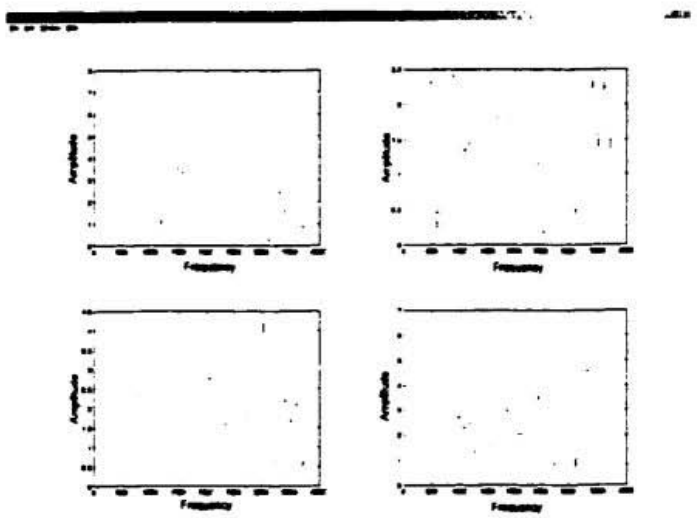

Figure B.3: Four Individual Z Components 0.51 m Resonance Data (Set 1)

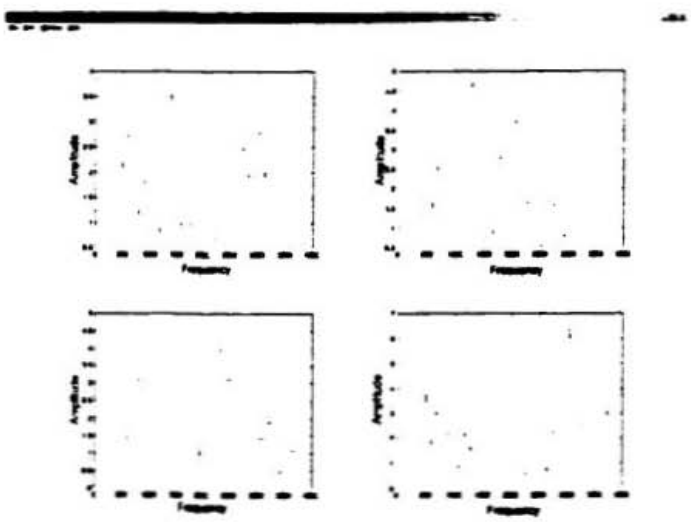

Figure B.4: Four Individual Z Components 0.51 m Resonance Data (Set 2)

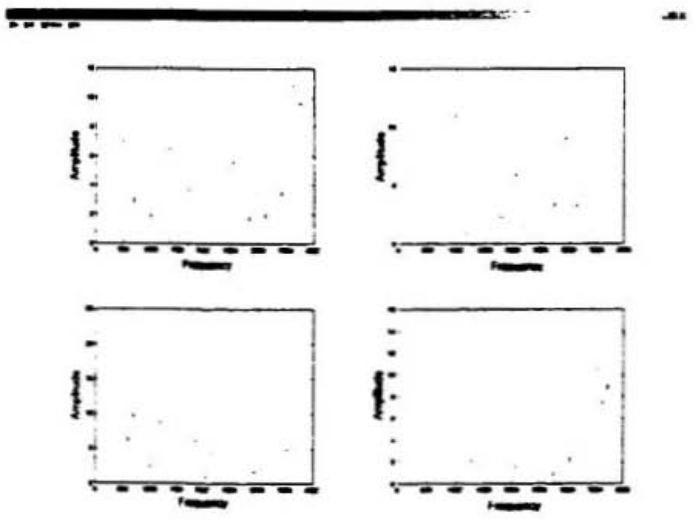

Figure B.5: Four Individual X Components 0.60 m Resonance Data (Set 1)

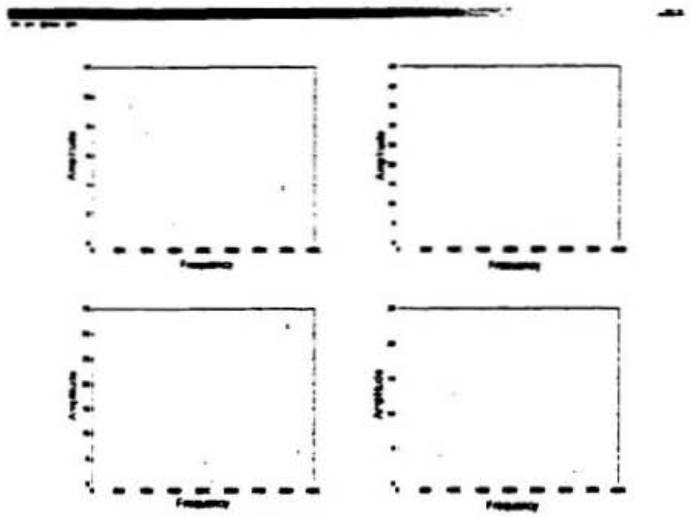

Figure B.6: Four Individual X Components 0.60 m Resonance Data (Set 2)

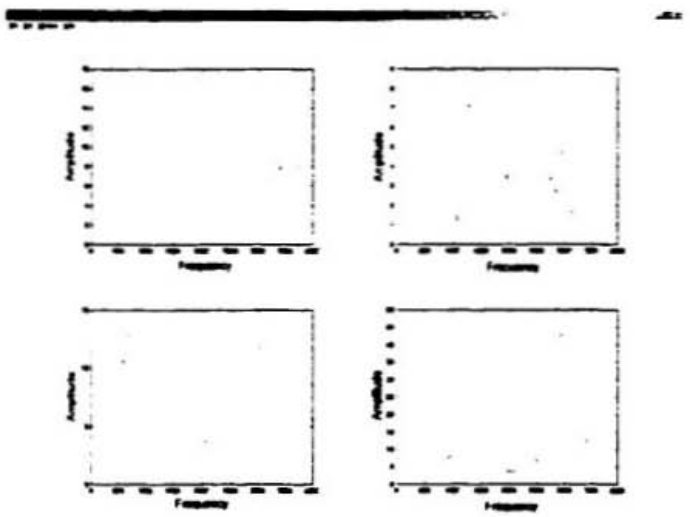

Figure B.7: Four Individual Z Components 0.60 m Resonance Data (Set 1)

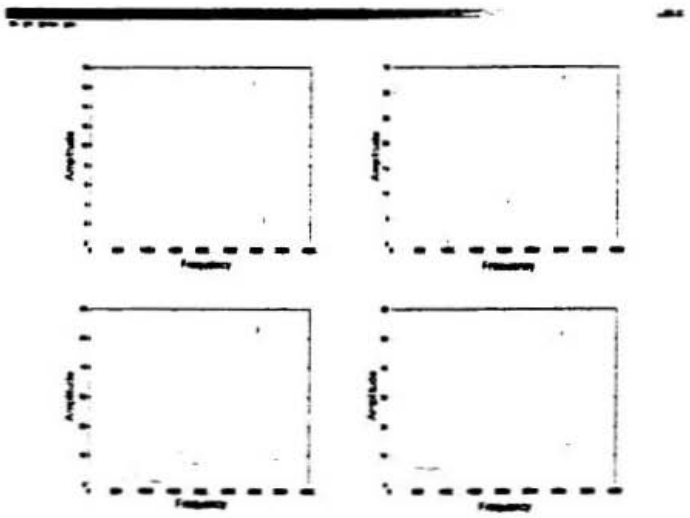

Figure B.8: Four Individual Z Components 0.60 m Resonance Data (Set 2)

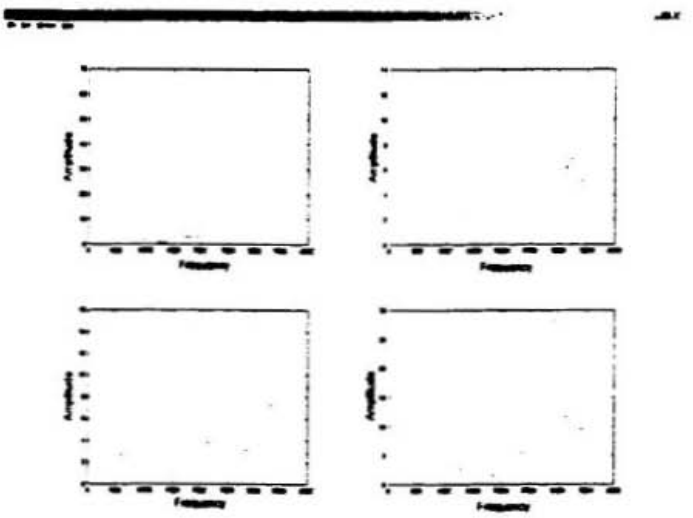

Figure B.9: Four Individual X Components 0.71 m Resonance Data (Set 1)

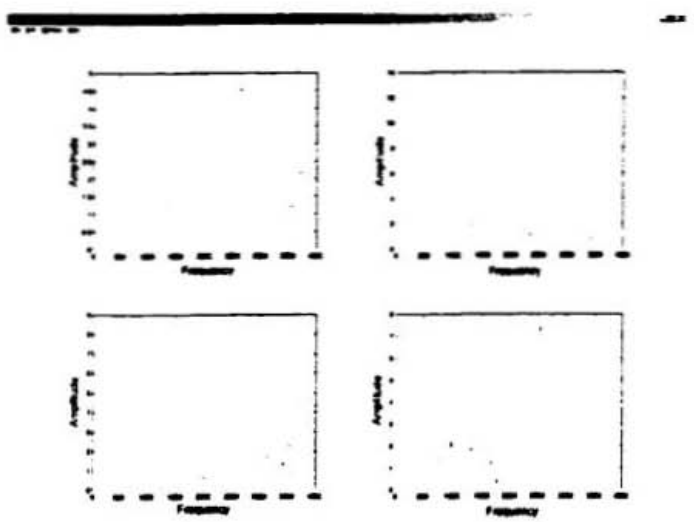

Figure B.10: Four Individual X Components 0.71 m Resonance Data (Set 2)

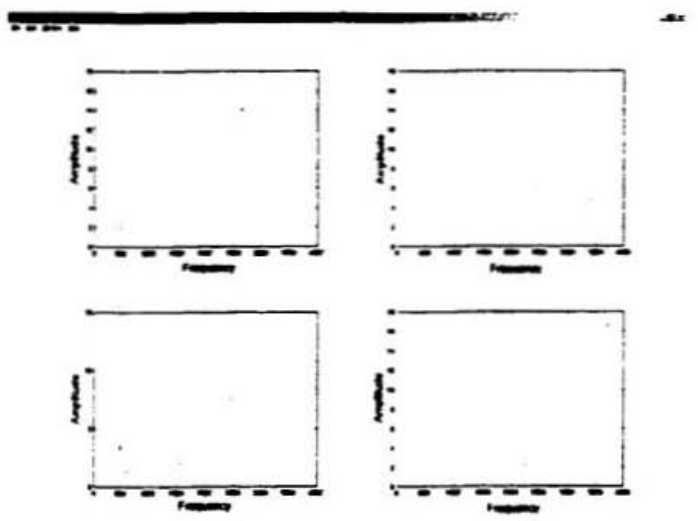

Figure B.11: Four Individual Z Components 0.71 m Resonance Data (Set 1)

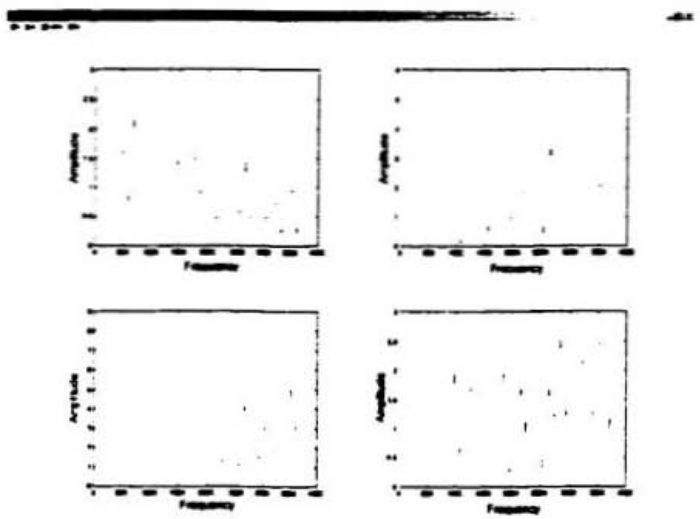

Figure B.12: Four Individual Z Components 0.71 m Resonance Data (Set 2)

Appendix C

Transducer Circuitry

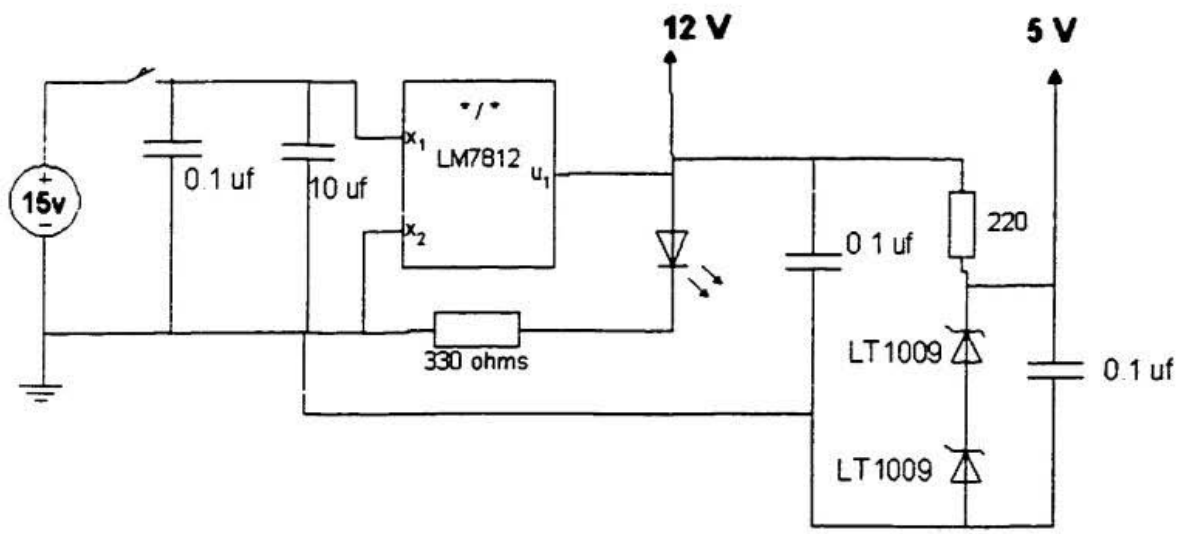

Figure C.1: Transducer Power Supply

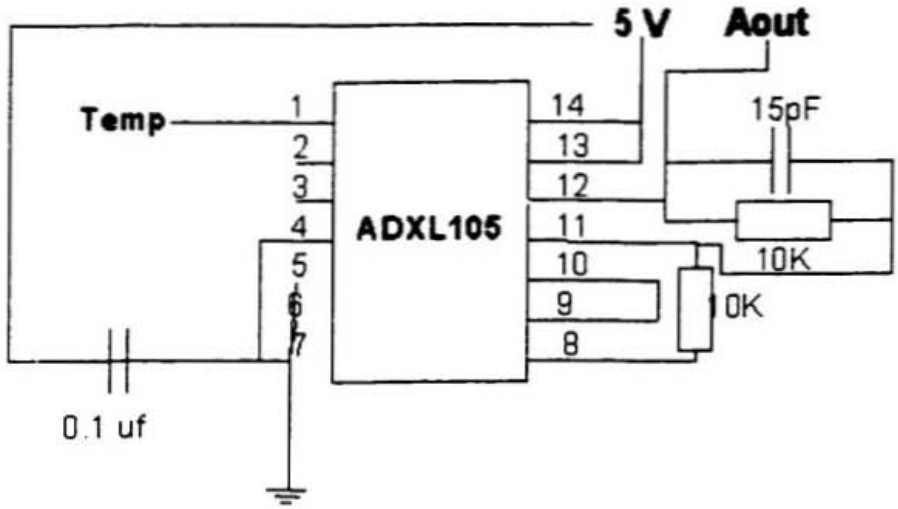

Figure C.2: Transducer Main Circuit

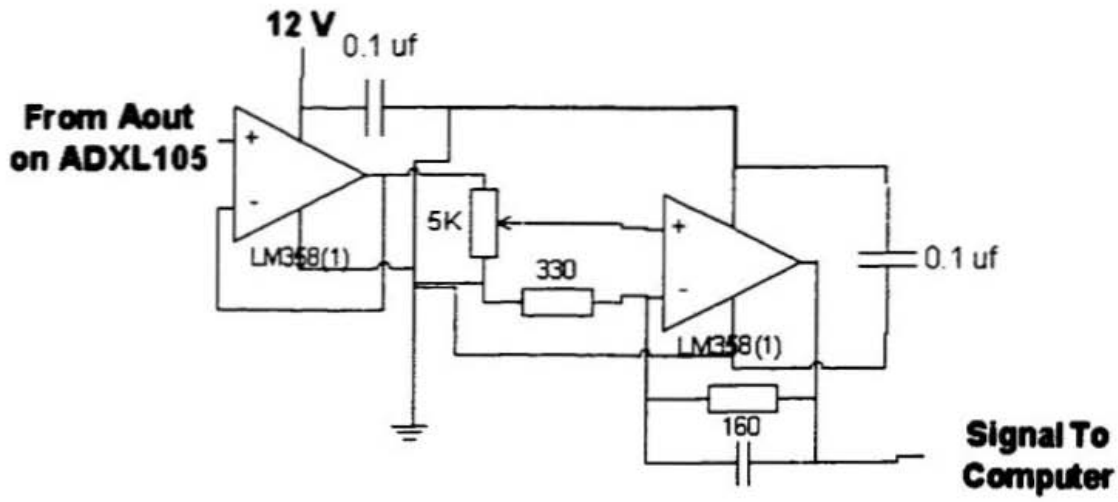

Figure C.3: Transducer Impedance Reduction For Long Cable Noise Reduction

Appendix D

ADXL105 Data Sheet

High Accuracy ±1 *g* to ±5 *g* Single Axis *i*MEMS® Accelerometer with Analog Input

ADXL105*

FEATURES
Monolithic IC Chip
2 *m*g Resolution
10 kHz Bandwidth
Flat Amplitude Response (±1%) to 5 kHz
Low Bias and Sensitivity Drift
Low Power 2 mA
Output Ratiometric to Supply
User Scalable *g* Range
On-Board Temperature Sensor
Uncommitted Amplifier
Surface Mount Package
+2.7 V to +5.25 V Single Supply Operation
1000 *g* Shock Survival

APPLICATIONS
Automotive
Accurate Tilt Sensing with Fast Response
Machine Health and Vibration Measurement
Affordable Inertial Sensing of Velocity and Position
Seismic Sensing
Rotational Acceleration

FUNCTIONAL BLOCK DIAGRAM

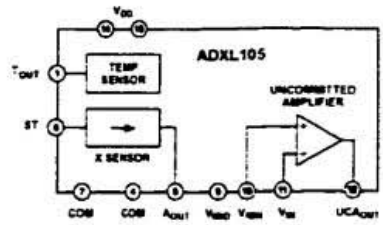

GENERAL DESCRIPTION

The ADXL105 is a high performance, high accuracy and complete single-axis acceleration measurement system on a single monolithic IC. The ADXL105 offers significantly increased bandwidth and reduced noise versus previously available micromachined devices. The ADXL105 measures acceleration with a full-scale range up to ±5 *g* and produces an analog voltage output. Typical noise floor is 225 $\mu g/\sqrt{Hz}$ allowing signals below 2 *m*g to be resolved. A 10 kHz wide frequency response enables vibration measurement applications. The product exhibits significant reduction in offset and sensitivity drift over temperature compared to the ADXL05.

The ADXL105 can measure both dynamic accelerations, (typical of vibration) or static accelerations (such as inertial force, gravity or tilt).

Output scale factors from 250 mV/*g* to 1.5 V *g* are set using the on-board uncommitted amplifier and external resistors. The device features an on-board temperature sensor with an output of 8 mV/°C for optional temperature compensation of offset vs. temperature for high accuracy application.

The ADXL105 is available in a hermetic 14-lead surface mount Cerpak with versions specified for the 0°C to +70°C, and −40°C to +85°C temperature ranges.

*Patent Pending.
iMEMS is a registered trademark of Analog Devices, Inc.

REV. A

One Technology Way, P.O. Box 9106, Norwood, MA 02062-9106, U.S.A.
Tel: 781/329-4700 World Wide Web Site: http://www.analog.com
Fax: 781/326-8703

ADXL105—SPECIFICATIONS ($T_A = T_{min}$ to T_{max}, $T_A = +25°C$ for J Grade Only, $V_S = +5$ V, @ Acceleration = 0 g, unless otherwise noted)

Parameter	Conditions	ADXL105J/A Min	Typ	Max	Units
SENSOR INPUT					
Measurement Range[1]		±5	±7		g
Nonlinearity	Best Fit Straight Line		0.2		% of FS
Alignment Error[2]			±1		Degrees
Cross Axis Sensitivity[3]	Z Axis, @ +25°C		±1	±5	%
SENSITIVITY[4] (Ratiometric)	At A_{OUT}				
Initial		225	250	275	mV/g
	V_S = 2.7 V	80	105	120	mV/g
vs. Temperature[5, 6]			±0.5		%
ZERO g BIAS LEVEL[4] (Ratiometric)	At A_{OUT}				
Zero g Offset Error	From +2.5 V Nominal	±25		+625	mV
vs. Supply		20		+25	mV/V, V
vs. Temperature[5, 6]			80		mV
NOISE PERFORMANCE					
Voltage Density[7]	@ +25°C		225	525	μg/√Hz
Noise in 100 Hz Bandwidth			2.25		mg rms
FREQUENCY RESPONSE					
3 dB Bandwidth		10	12		kHz
Sensor Resonant Frequency		13	18		kHz
TEMP SENSOR[8] (Ratiometric)					
Output Error at +25°C	From +2.5 V Nominal	100		+100	mV
Nominal Scale Factor			8		mV/°C
Output Impedance			10		kΩ
V_{REF}[9] (Ratiometric)					
Output Error	From +2.5 V Nominal	15		+15	mV
Output Impedance			1.0		kΩ
SELF-TEST (Proportional to V_{REF})					
Voltage Delta at A_{OUT}	Self-Test "0" to "1"	100		500	mV
Input Impedance[10]		30	50		kΩ
A_{OUT}					
Output Drive	I = ±50 μA	0.50		V_S − 0.5	V
Capacitive Load Drive		1000			pF
UNCOMMITTED AMPLIFIER					
Initial Offset		25		+25	mV
Initial Offset vs. Temperature			5		μV/°C
Common-Mode Range		1.0		1.0	V
Input Bias Current[11]			25		nA
Open Loop Gain			100		V/mV
Output Drive	I = ±100 μA	0.25		V_S − 0.25	V
Capacitive Load Drive		1000			pF
POWER SUPPLY					
Operating Voltage Range		2.70		5.25	V
Quiescent Supply Current	At 5.0 V		1.6	2.6	mA
	At 2.7 V		1.3	2.0	mA
Turn-On Time			700		μs
TEMPERATURE RANGE					
Operating Range J		0		+70	°C
Specified Performance A		−40		+85	°C

NOTES

[1] Guaranteed by tests of zero g bias, scale factor and output swing.

[2] Alignment of the X axis is with respect to the long edge of the bottom half of the ceramic package.

[3] Cross axis sensitivity is measured with an applied acceleration in the Z axis of the device.

[4] This parameter is ratiometric to the supply voltage V_{DD}. Specification is shown with a 5.0 V V_{DD}. To calculate approximate values at another V_{DD} multiply the specification in V_{DD} * V.

[5] Specification refers to the maximum change in parameter from its initial value at +25°C to its worst case value at T_{MIN} to T_{MAX}.

[6] See Figure 1.

[7] See Figure 2.

[8] CMOS and TTL Compatible.

[9] V_{REF} input bias current is tested at final test.

All min and max specifications are guaranteed. Typical specifications are not tested or guaranteed.

Specifications subject to change without notice.

ABSOLUTE MAXIMUM RATINGS*

Acceleration (Any Axis, Unpowered for 0.5 ms) ..... 1000 *g*
Acceleration (Any Axis, Powered for 0.5 ms) ..... 500 *g*
$+V_S$ ..... -0.3 V to +7.0 V
Output Short Circuit Duration
(Any Pin to Common) ..... Indefinite
Operating Temperature ..... -55°C to +125°C
Storage Temperature ..... -65°C to +150°C

*Stresses above those listed under Absolute Maximum Ratings may cause permanent damage to the device. This is a stress rating only; the functional operation of the device at these or any other conditions above those indicated in the operational sections of this specification is not implied. Exposure to absolute maximum rating conditions for extended periods may affect device reliability.

Package Characteristics

Package	θ_{JA}	θ_{JC}	Device Weight
14-Lead Cerpak	110°C/W	30°C/W	<2 Grams

ORDERING GUIDE

Model	Temperature Range	Package Option
ADXL105JQC	0°C to +70°C	QC-14
ADXL105AQC	-40°C to +85°C	QC-14

CAUTION

ESD (electrostatic discharge) sensitive device. Electrostatic charges as high as 4000 V readily accumulate on the human body and test equipment and can discharge without detection. Although the ADXL105 features proprietary ESD protection circuitry, permanent damage may occur on devices subjected to high energy electrostatic discharges. Therefore, proper ESD precautions are recommended to avoid performance degradation or loss of functionality.

Drops onto hard surfaces can cause shocks of greater than 1000 *g* and exceed the absolute maximum rating of the device. Care should be exercised in handling to avoid damage.

PIN FUNCTION DESCRIPTIONS

Pin No.	Name	Description
1	T_{OUT}	Temperature Sensor Output
2, 3, 5	NC	No Connect
4	COM	Common
6	ST	Self-Test
7	COM	Common (Substrate)
8	A_{OUT}	Accelerometer Output
9	V_{REF}	$V_{DD}/2$ Reference Voltage
10	V_{AIN}	Uncommitted Amp Noninverting Input
11	V_{IN}	Uncommitted Amp Inverting Input
12	UCA_{OUT}	Uncommitted Amp Output
13, 14	V_{DD}	Power Supply Voltage

PIN CONFIGURATION

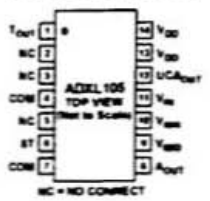

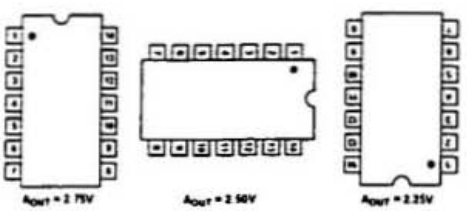

Figure 1. ADXL105 Response Due to Gravity

Appendix E

Simulator Matlab Code

```
clear all

%simulator for transducers on ice sheet
%mike wrinch, april 2001

%%%%%%%%%%%%%%%%%%%%%%
%input structure:
%%%%%%%%%%%%%%%%%%%%%%

    computer=struct('sampling_frequency',200000,'sampled_points',5000)

    computer.sampling_frequency=200000;
    computer.sampled_points=5000;

    signal=struct('frequency',0,'amplitude',0,'array',zeros(1,computer.sampled_points));

    noise=struct('A',signal,'B',signal,'C',signal,'D',signal,'white',signal)
    ice=struct('depth',0.70,'temperature',-15,'velocity',3750)
    transducer=struct('hammer_to_trans1',0.7,'trans1_to_trans2',0.7)

    time_array=zeros(1,computer.sampled_points);
        for i=1:computer.sampled_points
            time_array(i)=i*(1/computer.sampling_frequency);
        end

    noise_shape=struct('rise_time',0.0002,'rise_location',1,'decay_time',0.001,'decay_location'
    ,0.0125,'envelope',zeros(1,computer.sampled_points));

%%%%%%%%%%%%%%%%%%%%%%
%input variables:
%%%%%%%%%%%%%%%%%%%%%%

    computer.sampling_frequency=200000;
    computer.sampled_points=5000;

    ice.depth=0.7
    ice.temperature=-15
    ice.velocity=3750

    transducer.hammer_to_tran1=0.5
    transducer.trans1_to_trans2=0.5
```

```
    noise_shape.rise_time=0.00060 %0.0002
    noise.shape.rise_location=1
    noise_shape.decay_time=0.00250
    noise_shape.decay_location=noise.shape.rise_location+300

    noise.A.frequency=6000;
    noise.A.amplitude=.8;
    noise.A.array=sin(time_array*2*pi*noise.A.frequency)*noise.A.amplitude

    noise.B.frequency=7000;
    noise.B.amplitude=.6;
    noise.B.array=sin(time_array*2*pi*noise.B.frequency)*noise.B.amplitude

    noise.C.frequency=14500;
    noise.C.amplitude=0.25;
    noise.C.array=sin(time_array*2*pi*noise.C.frequency)*noise.C.amplitude

    noise.D.frequency=17500;
    noise.D.amplitude=1;
    noise.D.array=sin(time_array*2*pi*noise.D.frequency)*noise.D.amplitude

%%%%%%%%%%%%%%%%%%%%%%
% white noise building
%%%%%%%%%%%%%%%%%%%%%%

    noise.white.amplitude=0.025
    white=randn(1,computer.sampled_points);
    noise.white.array=(white/(max(white)))*noise.white.amplitude;

%%%%%%%%%%%%%%%%%%%%%%
%building of signal
%signal is one cycle of some unknown f at some unknown amplitude.
%%%%%%%%%%%%%%%%%%%%%%

    pulse=signal;   %hammer strike simulation
    pulse.frequency=5000; %determined from actural data calculations
    pulse.amplitude=1;
    pulse.decay_time=0.0001;
    pulse.array=sinc(pi/4-time_array*2*pi*pulse.frequency)*pulse.amplitude;
    %   pulse.array=exp(-((time_array)/pulse.decay_time)).*
    sin(time_array*2*pi*pulse.frequency)*pulse.amplitude;

    resonance=signal; % resonance simulation
    resonance.decay_time=0.00150;
    resonance.frequency=ice.velocity/(2*ice.depth);
    resonance.amplitude=.1;
    resonance.array=exp(-((time_array)/resonance.decay_time)).*
    sin(time_array*2*pi*resonance.frequency)*resonance.amplitude;

    first_arrival=signal;
    first_arrival.amplitude=1;

    offset=0;
    count=1;
    for i=1:length(first_arrival.array)
        if i>offset
            first_arrival.array(i)=pulse.array(count)*first_arrival.amplitude;
            count=count+1;
        end
    end
```

```
    first_reflection=signal;
    first_reflection_arrival_time=(2*(sqrt(ice.depth^2+
    (0.5*transducer.hammer_to_tran1)^2))-transducer.hammer_to_tran1)/ice.velocity
    first_reflection.amplitude=first_arrival.amplitude*.5 %decay of reflection

    offset=(first_reflection_arrival_time*200000)% time calculated from ice depth;
    count=1;

    for i=1:length(first_reflection.array)
        if i>offset
            first_reflection.array(i)=pulse.array(count)*first_reflection.amplitude;
            count=count+1;
        end
    end


%%%%%%%%%%%%%%%%%%%%%%
%envelope building (gaussian shape)
%%%%%%%%%%%%%%%%%%%%%%

    rise_gaussian=1-exp(-(time_array/noise_shape.rise_time).^2);
    decay_gaussian=exp(-((time_array)/noise_shape.decay_time).^2);

    count=1;
    while count<computer.sampled_points
        if (count>=noise_shape.rise_location)&(count<=noise_shape.rise_location+399)
            for i=1:400
                noise_shape.envelope(count)=rise_gaussian(i);
                count=count+1;
            end
        end
        if (count>=(noise_shape.rise_location+400))&(count<=noise_shape.decay_location)
            noise_shape.envelope(count-1)=1;

        end

        if count>=noise_shape.decay_location
            temp=count;
            for i=1:computer.sampled_points-temp
                noise_shape.envelope(count-1)=decay_gaussian(i);
                count=count+1;
            end

        end
        count=count+1;
    end %while

%%%%%%%%%%%%%%%%%%%%%%
%building of signal with corruption signal from generated noise
%%%%%%%%%%%%%%%%%%%%%%

    actual_signal=first_arrival.array+first_reflection.array+resonance.array;
    noise_total=noise.A.array+noise.B.array+noise.C.array+noise.D.array;
    corrupting_noise=(((noise_total).*
    noise_shape.envelope)+actual_signal+noise.white.array);%+resonance.array);

%%%%%%%%%%%%%%%%%%%%%%
% signal analysis (FFT)
%%%%%%%%%%%%%%%%%%%%%%
    n=2048;          %analized_signal_size
    HAMMING=hamming(n);
    temp_signal=corrupting_noise(1:n);
```

```
    for I=1:n,
        temp_signal(I)=HAMMING(I)*temp_signal(I); %windowing.
    end

    frequency_domain=abs(fft(temp_signal));
    frequency_range=20000;
    plot_area=int32(frequency_range/(computer.sampling_frequency/(2*n)));
    freq=zeros(n,1);

    for I=1:n,
        freq(I)=(I-1)*(200000/n);
    end

%%%%%%%%%%%%%%%%%%%%%%
%% reflection time
%%%%%%%%%%%%%%%%%%%%%%

ttfr=(2*(sqrt((transducer.hammer_to_tran1/2)^2+ice.depth^2))/ice.velocity)*
computer.sampling_frequency;

ttfr2=((2*(sqrt((transducer.hammer_to_tran1/2)^2+ice.depth^2))/ice.velocity)-
transducer.hammer_to_tran1/ice.velocity)*computer.sampling_frequency;


%%%%%%%%%%%%%%%%%%%%%
% signal analysis FIR1
%%%%%%%%%%%%%%%%%%%%%


    fir_filter=struct('poles',1,'frequency_low',1,'frequency_high',1,'B',0,'frequ2pi_ref',0);

    fir_filter.poles=500;
    fir_filter.frequency_high=6500;     %Hz
    fir_filter.frequency_low=190;   %Hz

    fir_filter.frequ_high2pi_ref=(2*fir_filter.frequency_high)/computer.sampling_frequency;
    fir_filter.frequ_low2pi_ref=(2*fir_filter.frequency_low)/computer.sampling_frequency;
    fir_filter.B=fir1(fir_filter.poles,[fir_filter.frequ_low2pi_ref,fir_filter.frequ_high2pi_ref])


    n=2048;
    filtered_signal=filter(fir_filter.B,1,corrupting_noise);

    temp_signal=filtered_signal(1:n);

    for I=1:n,
        temp_signal(I)=HAMMING(I)*temp_signal(I); %windowing.
    end

    frequency_filtered_signal=abs(fft(temp_signal));

%%%%%%%%%%%%%%%
%cross correlation
%%%%%%%%%%%%%%%

x1corr=xcorr(filtered_signal,filtered_signal);
x2corr=xcorr(filtered_signal,filtered_signal);

%%%%%%%%%
%plots
%%%%%%%%%
```

```
subplot(231),plot(first_arrival.array(0:300)),title('first arrival'),
  xlabel('Samples');
subplot(232),plot(freq(0:200),frequency_domain(0:200)),title
   ('Frequency analysis of sensor resonance'),xlabel('Frequency');
subplot(233),plot(noise_shape.envelope(0:1900)),title
    ('Sensor Resonance Decay Envelope'),xlabel('Samples');
subplot(234),plot(corrupting_noise(0:1700)),title
    ('Result Noise/Resonance with envelope'),xlabel('Samples');
subplot(235),plot(first_reflection.array(0:299)+
   first_arrival.array(0:299)),title('first arrival +
    first reflection'),xlabel('Samples');
subplot(236),plot(freq(0:200),corrupting_noise(0:200)),title
    ('first reflection'),xlabel('Samples');

%subplot(236),plot(first_reflection.array(0:299)),
%   title('first reflection'),xlabel('Samples');
%subplot(2,1,1), cwt(filtered_signal(200:500),1:120,
%  'db5','wavelet of corrupting noise');
%subplot(2,1,2), plot(filtered_signal(200:500)),
%   title('Result Noise/Resonance with envelope'),
%  xlabel('Samples');
%subplot(313),plot(x2(68,1:199)),title(' wavelette 25')
%subplot(221),plot(freq(0:200),frequency_domain(0:200)),title
%  ('Frequency analysis of sensor resonance'),
% xlabel('Frequency');
%subplot(222),plot(freq(0:200),frequency_filtered_signal(0:200)),
% title('Frequency analysis of sensor resonance'),xlabel('Frequency');
%plot(sinc(pi/2-time_array(1:200)*2*pi*noise.A.frequency))
%subplot(111), plot(xlcorr(3999:6000));
```

References

[1] E. Lewis. "Review of foating ice thickness measurement." department of fisheries and oceans. Canplar Consultants Ltd.. Jan. 1985.

[2] C. H. Yew. "Use of penetrators to estimate the properties of ice in the arctic region." in *Arctic Oceanography Conference and Workshop*. 1985.

[3] M. Langeleben and E. Pounder. "Acoustic attenuation in sea ice." ice research project. Macdonald Physics Laboratory McGill University. May 1970.

[4] D. M. Farmer and Y. Xie. *Remote Sensing of Sea Iceand Icebergs*. ch. 3. pp. 97–130. New York New York: John Wiley and Sons. Inc.. 1994.

[5] D. M. Farmer and Y. Xie. "The sound generated by propagating cracks in sea ice." *Acoustical Society of America*. vol. 85. pp. 1489–1500. July 1989.

[6] K. L. Williams. R. Stein. T. Wen. and R. E. Francois. "Determination of elastic moduli of sea ice." in *Oceanus*. pp. 1231–1235. Sept. 1989.

[7] N. K. Sinha. "Grain-size influence on effecture modulus of ice." in *Workshop on Bearing Capacity of Ice Coverage*. pp. 65–74. Oct. 1978.

[8] G. E. Frankenstien. "Dynamic young's modulus and flexural strength of sea ice." cold regions research and engineering laboratory. United States Army. May 1970.

[9] T. R. Ringer. "Ultrasonic investigations of ice." low temperature laboratory. Canadian National Research Counsel Devision of Mechanical Engineering. Oct 1977.

[10] A. C. S. D. Kishoni. "Measurement of the speed of sound in ice." *American Insitute of Aeronautics and Astronautics*. vol. 24. pp. 1713–1715. feb 1986.

[11] M. P. Langleben. "Attenuation of sound in sea ice. 10-500 khz." *Journal of Glaciology*. vol. 8. pp. 399–406. 54.

[12] V. Bogorskii and A. Gusev. "Attenuation of sound in ice in the frequency range 200-1100 khz." *Soviet Physics and Acoustic*. vol. 19. pp. 97–100. September-October 1973.

[13] P. de Heering. "An impact sound source useful for arctic remote sensing." *IEEE Journal of Oceanic Engineering*. vol. 14(2). pp. 166–172. feb 1989.

[14] N. Sinha. "Acoustic emission and microcracking in sea ice." in *Japan Society for Mechanical Engineers*. 1982.

[15] V. gavrilo and A. Gusev. "Acoustic pulses produced by impact excitation of floating ice." *Chin*. vol. 1. p. 5. 1969.

[16] R. Sheriff and L. Geldart. *Exploration Siesmology*. ch. 1.2.3.4.5.6. pp. 1–400. The Pitt Building. Trupington Street. Cambridge.CB2 1RP: Cambridge University Press. 1995.

[17] M. J. Crocker. *Handbook of Acoustics*. ch. 6.15. pp. 547.1367. 605 Third Avenue. New York. New York: John Wiley and Sons. Inc.. 1998.

[18] J. Xiang. "High resolution siesmic imaging of the near-surface: Camparison of energy sources." Master's thesis. Memorial University of Newfoundland. Apr 2000.

[19] T. R. Morgan. *Foundations of Wave Theory for Seismic Exploration*. ch. 2. pp. 28–32. 137 Newbury Street. Boston. MA 02116: International Human Resources Development Corporation. 1997.

[20] B. Lathi. *Modern Digital and Analog Communication Systems*. ch. 2.7. pp. 40–45. 189 Madison Avenue. New York. New York. 10016: Oxford University Press. 1998.

[21] A. V. Oppenheim and A. S. Willsky. *Signals and Systems*. ch. 1.2.6.7. Upper Saddle River. New Jersey. 07458: Prentice Hall. 1997.

[22] M. Langeleben and E. Pounder. "Reflection of sound at the water-ice interface." ice research project. Macdonald Physics Laboratory McGill University. may 1970.

[23] A. V. Oppenheim and R. W. Schafer. *Discrete Time Signal Processing*. ch. 2.6.7.8. p. 0. Upper Saddle River. New Jersey. 07458: Prentice Hall. 1998.

[24] S. Timoshenko and J. Goodier. *Theory of Elasticity. Third ed. Engineering Society Monographs*. ch. All. p. All. New York: McGraw-Hill Book Company. 1970.